METHYLENE BLUE (MB) LOADED ZIF-8 SYNTHESIS, CHARACTERIZATION AND INVESTIGATION OF PHOTODYNAMIC THERAPY ACTIVITY ON BREAST CANCER

A Thesis Submitted to
the Graduate School of
İzmir Institute of Technology
in Partial Fulfilment of the Requirements for the Degree of

MASTER OF SCIENCE

in Chemistry

by
Pınar ÖZTÜRK

July 2024
İZMİR

We approve the thesis of **Pınar ÖZTÜRK**

Examining Committee Members:

Prof. Dr. Gülşah Şanlı MOHAMMED
Department of Chemistry, Izmir Institute of Technology

Prof. Dr. Yaşar AKDOĞAN
Department of Materials Science and Engineering, Izmir Institute of Technology

Assoc. Prof. Dr. Muhammed ÜÇÜNCÜ
Department of Pharmacy, Izmir Katip Celebi University

11 July 2024

Prof. Dr. Gülşah Şanlı MOHAMMED
Supervisor, Department of Chemistry,
Izmir Institute of Technology

Prof. Dr. Gülşah Şanlı MOHAMMED
Head of the Department of Chemistry

Prof. Dr. Mehtap EANES
Dean of the Graduate School of
Engineering and Sciences

ACKNOWLEDGMENTS

First and foremost, I want to thank Prof. Dr. Gülşah Şanlı Mohamed for the incredible opportunity to join the biochemistry research group and its projects. Her support, incredible smile, and the energy she brings have given me invaluable perspectives and lessons. I am especially grateful for her understanding and the space she provided for me to express my ideas and reach my potential. She was my greatest fortune.

I would also like to express my appreciation to my thesis committee, Assoc. Prof. Dr. Muhammed ÜÇÜNCÜ and Prof. Dr. Yaşar AKDOĞAN for accepting to evaluate my thesis and their valuable suggestions.

I would like to thank all the staff and facility managers at IYTE MAM and BIYOMER for their kind assistance and suggestions.

I am grateful to Dr. Derya METE for being not only a teacher and guide but also the best lab partner I could ask for. Her beautiful smile, positive energy, belief in me, patience, and support under all circumstances made this journey truly special. I would like to thank the members of the GSM Biochemistry Laboratory for their support and guidance.

My special thanks go to my family members Gülperi ÖRNEK, Mehmet ÖZTÜRK, Çağla ÖZTÜRK. I extend my heartfelt thanks to my mother for reminding me how amazing it is when a mother believes in and supports her daughter. I owe the greatest thanks in this thesis to my dear sister, the secret hero of this journey. I am deeply grateful for her constant support, unconditional love, and patience, and never letting go of my hand no matter what. Thank you, my wonderful sister, for being my greatest blessing and always being by my side every step of the way with our joy JOEY.

I would also like to thank my second family Buse TÜTÜNCÜ, Selen DAL, Beyza TUNÇ, Böke ARABACI, İlyas Yasin ÇİFTÇİ, Miray CEBECİ, Ece TOPCU, Mehmetcan ÖZTÜRK, Mustafa KANDEMİR and Ecem ONUK for making this process fulfilling with their endless belief, support, and love for me.

This study was supported by the Scientific and Technological Research Council of Turkey (TÜBİTAK, 118C596)

ABSTRACT

METHYLENE BLUE (MB) LOADED ZIF-8 SYNTHESIS, CHARACTERIZATION AND INVESTIGATION OF PHOTODYNAMIC THERAPY ACTIVITY ON BREAST CANCER

Although various methods are used today in the diagnosis and treatment of breast cancer, traditional approaches have disadvantages such as drug resistance, drug cytotoxicity, metastasis, and relapse. Therefore, new methods need to be developed for early diagnosis of the disease and improvement of the treatment process. Photodynamic diagnosis and therapy have gained importance in this context in recent years.

The primary purpose of this study was to use metal-organic frameworks for the first time to include methylene blue in the breast cancer treatment process with photodynamic therapy. The nano-delivery system using methylene blue was examined for its cytotoxic effect on breast cancer cell lines MDA-MB-231 and MCF-7. Since ZIF-8 degrades and provides zinc to cells, this material was expected to have an additional therapeutic property alongside photodynamic therapy. In addition, the combination of multiple cytotoxic components in a single nanoparticle and their combined effects was evaluated. The new generation nanocarriers were designed to release methylene blue specifically in cancer cells with low pH, avoiding damage to healthy tissues and enhancing the quality of the treatment process.

ÖZET

METİLEN MAVİSİ (MM) YÜKLÜ ZIF-8 SENTEZİ, KARAKTERİZASYONU VE MEME KANSERİNDE FOTODİNAMİK TEDAVİ ETKİNLİĞİNİN İNCELENMESİ

Günümüzde meme kanserinin teşhis ve tedavisinde çeşitli yöntemler kullanılmasına rağmen, geleneksel yöntemlerin ilaç direnci, ilaç sitotoksisitesi, metastaz ve nüks gibi dezavantajları vardır. Bu nedenle, hastalığın erken teşhisi ve tedavi sürecinin iyileştirilmesi için yeni yöntemler geliştirilmesi gerekmektedir. Fotodinamik tanı ve tedavi, son yıllarda bu bağlamda önem kazanan bir yaklaşımdır.

Bu çalışmanın temel amacı, metal-organik iskeleleri ilk kez fotodinamik tedavi ile birlikte metilen mavisinin meme kanseri tedavi sürecine dahil etmek için kullanmaktır. Metilen mavisi kullanılan nano-taşıma sistemi, meme kanseri hücre hatları MDA-MB-231 ve MCF-7 üzerindeki sitotoksik etkisi açısından incelenmiştir. ZIF-8'in bozunarak hücrelere çinko sağlaması nedeniyle, bu malzemenin fotodinamik tedaviye ek olarak terapötik bir özellik göstermesi beklenmiştir. Ayrıca, tek bir nanopartikül içerisinde birden fazla sitotoksik bileşenin birleştirilmesi ve bunların kombine etkileri değerlendirilmiştir. Yeni nesil nano taşıyıcılar, metilen mavisini düşük pH'a sahip kanser hücrelerinde spesifik olarak salmak üzere tasarlanmış olup, sağlıklı dokulara zarar vermekten kaçınılarak tedavi sürecinin kalitesinin artırılması hedeflenmiştir.

TABLE OF CONTENTS

LIST OF FIGURES

Figure **Page**

Figure **Page**

LIST OF TABLES

Table **Page**

CHAPTER 1

INTRODUCTION

1.1. Cancer

Cancer is the uncontrolled division, proliferation, and accumulation of cells in an organism. It is a condition influenced by various genetic, environmental, and lifestyle factors. It can affect people of all ages, environments, and backgrounds. It can affect only one organ or area or spread to distant body organs through the lymphatic system or blood circulation. (Fitzmaurice et al. 2015)

Cancer is multifactorial, and it is much more likely to be caused by environmental factors than hereditary factors. All cancers occur due to abnormalities in the DNA sequence. (Pavlopoulou, Spandıdos, and Mıchalopoulos 2015). While the rate of cancers occurring through genes transferred from parents, inherited cancers, is 10-15%, the remaining 85-90% are thought to be triggered by mutagens causing replication errors in the DNA of living cells throughout life. (Skıpper, Schabel, and Wılcox 1964)

Individuals can become predisposed to cancer by inheriting defects in tumor suppressor genes that usually prevent tumor development, along with additional contributions from carcinogens such as smoking or radiation. In some types of cancer, such as breast and ovarian cancer, some genes have been identified in studies on the hereditary transmission of cancer. (Richie and Swanson 2003) In the absence of a mechanism to correct errors that may occur in the DNA structure of the cell, new mutations will be added to existing mutations after each cell division (because DNA will replicate itself). Since there is no mechanism to repair the damage that has begun, it will soon lead to metastases (Richie and Swanson 2003).

Cancer cells can resist harsh conditions such as low oxygen and limited nutrients, and over time, they can turn these conditions to their advantage, survive, and multiply. While normal cells can grow by attaching to a specific surface and survive with sufficient oxygen and nutrients, cancer cells can live, grow, and multiply without attaching to any surface (Leon-Ferre et al. 2018).

Metastasis symptoms occur when cancer develops in a specific area and spreads to other body parts through various processes. These may include enlarged lymph nodes, hepatomegaly or splenomegaly that can be felt in the abdomen, pain or fractures in affected bones, and neurological symptoms. Most cancer deaths are due to cancer that has spread (metastasized) from its primary site to other organs (Pavlopoulou, Spandıdos, and Mıchalopoulos 2015).

In addition to all this, it should be noted that different types of cancer have different effects (Richie and Swanson 2003). Although there are no definitive standards, different approaches and treatments are applied to each type of cancer. (Fitzmaurice et al. 2015) More than 100 types of cancer are known to affect the human body. (Pavlopoulou, Spandıdos, and Mıchalopoulos 2015).

1.1.1. Breast Cancer

Breast cancer is the second most diagnosed cancer and the second leading cause of cancer-associated deaths for women worldwide (Bray et al. 2018). This type of cancer is caused by an abnormal growth of cells in the breast tissue, and it has many subtypes. Malignant tumors are cancerous and behave aggressively, with unlimited growth and invasion into other tissues.

The two most commonly diagnosed types are invasive ductal carcinoma and invasive lobular carcinoma (DeSantis et al. 2014). Invasive ductal carcinoma (IDC) is caused by the uncontrolled growth of cells that line the ducts in the breast. IDC often spreads into surrounding tissues and comprises about 70-80% of breast cancer cases. Invasive lobular carcinoma (ILC) is less common than IDC and may have different spreading patterns in the breast tissue, as cells spread from the breast lobules to surrounding tissues (Rakha et al. 2008). BRCA1 and BRCA2 are genes that significantly raise the risk of breast cancer when mutated (Mavaddat et al. 2013). Other risk factors for breast cancer include age, family history, use of hormone replacement therapy, alcohol consumption, and obesity (Key, Verkasalo, and Banks 2001).

In 2020, 2.6 million women were diagnosed with breast cancer, according to the International Agency for Research on Cancer (IARC) GLOBOCAN. Worldwide, in 2020, it is the most common cancer type, making it also the most frequently diagnosed cancer type in the world (Ferlay et al. 2021). While it occurs more often in women, both

men and women can develop breast cancer. Moreover, it is the leading cause of cancer-related mortality and has a high incidence rate (number of new cases) (Ferlay et al. 2021).

1.1.2. MCF-7 Cell Line

MCF-7 breast adenocarcinoma cell line [ER+ (human)] This estrogen-dependent growth, which reflected that of primary tumors, allows for the assessment of the effectiveness of hormone-based treatments (Soule et al. 1973), and the cell line is most frequently used in this context. MCF-7 cells are a well-established model for studying the growth-promoting effects of estrogen in breast cancer since they are hormone receptor-positive.

1.1.3. MDA-MB-231 Cell Line

The MDA-MB-231 cell line, also known as triple-negative breast cancer (TNBC), is a cell line of breast cancer that is negative for estrogen receptor (ER), progesterone receptor (PR), and HER2 receptors. This leads to an aggressive phenotype with a high level of metastasis of these cells (Cailleau, Olivé, and Cruciger 1978). MDA-MB-231 cells have an important role in resistance to treatment and metastasis research.

1.2. Photodynamic Therapy

Photodynamic therapy is a treatment method based on the concept that photosensitizers are stimulated by exposing them to light, resulting in the production of singlet oxygen or reactive oxygen species that cause damage in the area where they are introduced (Pethő et al. 2019). PDT is a non-invasive method approved by the FDA for treating many types of cancer, microbial infections, and similar diseases. Photodynamic therapy is advantageous over chemotherapy because it initially contains an inactive, harmless drug (PS) without light. This photosensitizer is then stimulated with focused light on the area, and by releasing singlet oxygen species from reactive oxygen species, it eliminates its target without causing damage to the surrounding healthy tissue. After its activity, it provides a healing process without leaving a scar (Tyrrell, Paterson, and

Curnow 2019). In addition, the treatment is a repeatable and low-cost procedure and offers the chance to be easily reapplied in case of cancer recurrence (Lamberti 2014). In addition to its promising potential and gains, certain developments are needed to obtain more effective results in photodynamic therapy. The application of multiple therapies by improving transport and selectivity can be an example (Rahimipour et al. 2003). The PDT treatment method, which currently causes damage to the tumor micro-vasculature, enables the Enhanced Permeability Retention (EPR) feature to be activated by the transport of PS with nanoparticles, thus increasing the efficiency of the treatment (Wang et al. 2016). The EPR effect causes more nanoparticle accumulation in tumors than in healthy cells by taking advantage of the damaged vascular tissue of cancerous cells. (Subhan et al. 2021). EPR has been studied for more than 30 years, and it has been determined that the concentrations of nanoparticles applied in tumor xenografts in animal models increase with the EPR effect (Subhan et al. 2021).

1.3. Metal-Organic Frameworks

Metal-organic skeletons (MOFs) are crystalline, hybrid, and nanoscale materials formed by the coordination-based self-assembly of polydentate bridged ligands with metal ions (Rowsell and Yaghi 2004). The advantages of MOFs include adjustable pore number and width, large but specific surface area, low crystal density, high biocompatibility, and bionic catalytic properties (Furukawa et al. 2013).This enables MOFs to exhibit extraordinary performance in biomedical applications. MOFs can be classified as standard (1st generation), functional (2nd generation), and smart (3rd generation) according to their crystalline or amorphous structure, development processes, and metal ions: zinc-based, zirconium-based, iron-based, or many other metal ion-based (Romanello et al. 2021).

1.4. Chemical Structure of ZIF-8

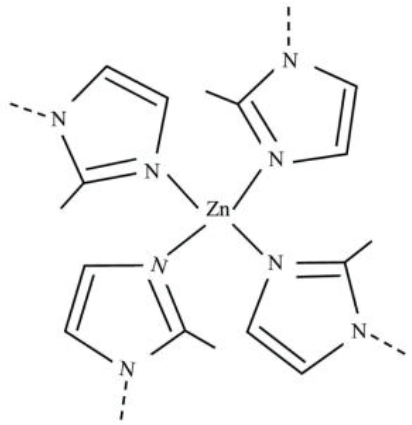

Figure 1. Chemical Structure of ZIF-8
(Source: Peng Chee et al. 2017)

Zeolite containing imidazole skeleton ZIF-8 is one of the most studied zinc-based MOF derivatives (Zou, Liu, and Zhang 2018). ZIF-8 is composed of zinc and 2-methylimidazole with sodalite (SOD) topology and has dense and large pores, high drug loading capacity, and excellent thermal and chemical stability in physiological environment. In addition, it has low pH-dependent degradation properties, such as in tumor microenvironment and endosomes, which are critically crucial against cancer (Xin et al. 2017). Commonly used drugs, such as doxorubicin, can be loaded onto ZIF-8 to deliver single or multiple chemotherapy agents (Akhtar et al. 2024). Additionally, photosensitizers like g-C3N4, Au25, and Pp IX are reported in the literature as photodynamic therapy (PDT) agents that are transported to cancerous tissues by ZIF-8 (Gao et al. 2019). It is known that zinc ion, which is a part of ZIF-8, is also given as an anti-cancer dietary supplement (Prasad et al. 2009). In addition, it has been recorded that high doses of zinc concentration cause ROS-induced apoptosis in human melanoma cells (Provinciali et al. 2015). For instance, "Sorafenib loaded ZIF-8 metal-organic frameworks as a multifunctional nano-carrier offers effective hepatocellular carcinoma therapy" (Mete, Yemeztaşlıca, and Şanlı-Mohamed 2023), highlighting the versatility and therapeutic potential of ZIF-8 in cancer treatment.

1.5. Chemical Structure of Methylene Blue

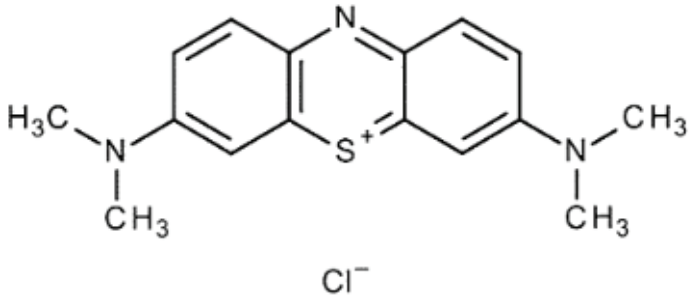

Figure 2. Chemical Structure of Methylene Blue
(Source: Tenhunen et al. 2018)

Methylene blue is a cheap, water-soluble, and non-toxic phenothiazine dye with a strong absorption peak at 550-700 nm, a maximum at 664 nm, and a strong photodynamic activity. Studies show singlet oxygen formation by methylene blue, a photosensitizer agent with well-known photochemical properties. (Fernandez, Bilgin, and Grossweiner 1997). After methylene blue binds to the target cell's mitochondrial membrane, PDT stimulation results in apoptotic cell death due to loss of mitochondrial function. In addition, methylene blue-PDT induces shrinkage in tumor cells due to binding to the negative electrochemical environment in the mitochondrial matrix (dos Santos et al. 2017). It has been reported that methylene blue-PDT mediates the induction of apoptosis by mitochondria-dependent pathways (Chen et al. 2008).

1.6. Cell Based Methods

The cell-based method is an essential tool in biomedical research to access cells' biological functions, including viability, cytotoxicity, apoptotic processes, biological activity, cell cycle, etc. These procedures have allowed detailed insight into the biological responses of cells and are a cornerstone of cancer research (Alley et al. 1988).

1.5.1. Cell Viability and Cytotoxicity Tests

Cell viability and cytotoxicity tests are essential tools in biomedical research, providing fundamental information about the health and functionality of cells under various conditions. These tests are essential in drug discovery, cancer research, and toxicity assessment, helping researchers determine the potential effects of compounds on cell health and survival (Alley et al. 1988).

Cell viability refers to the proportion of living, healthy cells in a population, while cytotoxicity measures the extent to which a substance can damage or kill cells. Various assays have been developed to assess these parameters, such as MTT, XTT, and trypan blue exclusion (Mosmann 1983). The choice of method should be compatible with the intended study.

The MTT test is a frequently used cell viability and cytotoxicity assessment methodology critical for many biomedical research areas. The MTT assay, initially described by Mosmann in 1983, represents a valid, quantitative tool to evaluate cell metabolic activity, which is strictly related to cell viability (Mosmann 1983). The MTT assay is made up of the water-soluble yellow compound MTT [3-(4,5-dimethylthiazol-2-yl)-2,5-diphenyltetrazolium bromide] that is reduced by mitochondrial succinate dehydrogenases of living cells to a water-insoluble purple formazan. This reaction is catalyzed by mitochondrial succinate dehydrogenase enzymes in functional mitochondria of the living cells (Berridge, Herst, and Tan 2005). Scheme 3. representation of the overall reaction.

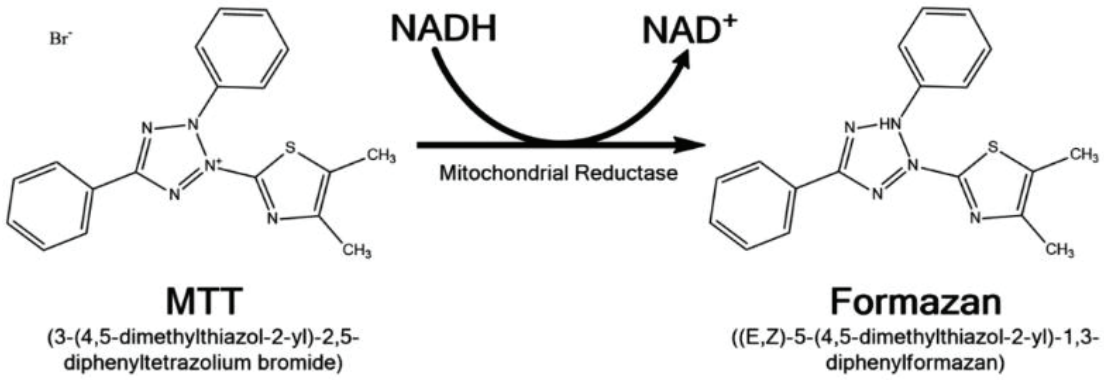

Figure 3. The chemical reaction of reduction to formazan

(Source:Kamiloglu et al. 2020)

In living cells, NADH produced during glycolysis and the tricarboxylic acid cycle acts as an electron donor by reducing the tetrazolium ring of MTT to form formazan crystals. This reduction is limited to metabolically active cells because dead cells do not have the enzymatic activity required for this action (Denizot and Lang 1986).

While it has some advantages, the MTT assay has limitations. Factors including cell density, incubation time, and the test compound, to name just a few of the many, affect each study (Fotakis and Timbrell 2006). Likewise, some compounds can prevent the MTT reduction, which can lead to false positive or false negative results. Solubilization can also be challenging as incomplete solubilization of formazan crystals causes absorbance readings to be inconsistent. Thus, optimizing and standardizing the experimental conditions in detail is necessary.

1.5.1. Cell Apoptosis

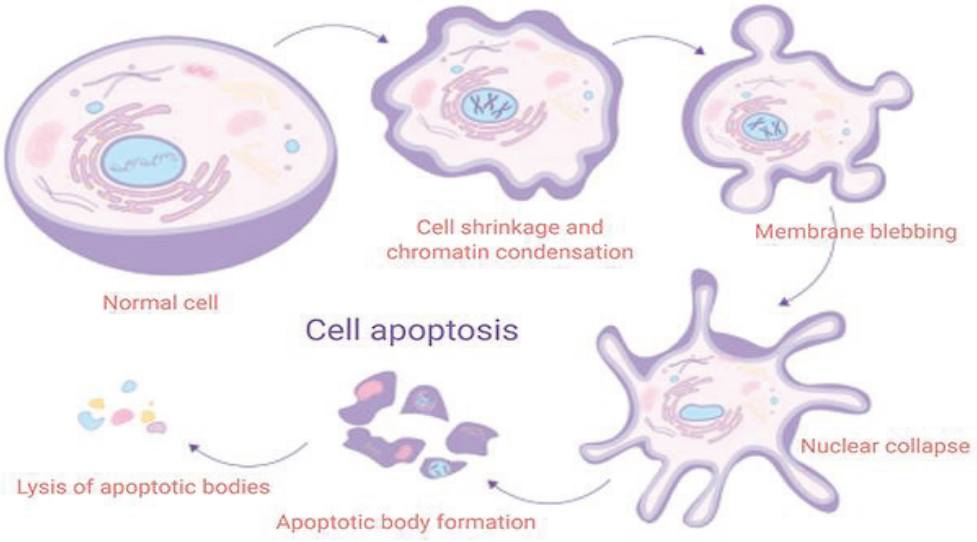

Figure 4. The Process of Apoptosis
(Source: MedChemExpress, n.d.)

Programmed cell death, or apoptosis, is necessary in multicellular organisms to remove damaged or undesired cells and preserve tissue homeostasis. Apoptosis is a highly regulated and controlled mechanism that permits cells to die without inducing an inflammatory response, in contrast to necrosis, a catastrophic form of cell death brought on by acute cellular injury (Kerr, Wyllie, and Currie 1972).

A pathological type of cell death known as necrosis typically results from an external stimulus such as an injury, an infection, or toxins. The swelling of cells brings on an inflammatory response, the rupture of plasma membranes, and the discharge of cell contents into the surrounding tissues. (Galluzzi et al. 2014). The main difference between apoptosis and necrosis is that necrosis is an uncontrolled cell death process, leading to tissue damage.

Apoptosis is significant for immunological response, development, and cancer prevention. It removes superfluous cells, like the ones between developing fingers and toes, during embryogenesis to shape organs and tissues (Penaloza et al. 2006). Apoptosis in the immune system clears activated lymphocytes following infection and removes autoreactive T cells to prevent autoimmune disorders (Strasser, O'Connor, and Dixit 2000). Additionally, the tumor suppressor protein p53 triggers apoptosis in response to cellular stress, acting as a barrier against cancer by eradicating cells that have oncogenic mutations or damaged DNA (Vousden and Lane 2007). Tumor formation can result from disruption of apoptosis because injured cells multiply excessively and avoid death.

This process involves a series of distinct morphological and biochemical changes. Initially, cells undergo shrinkage, and their membranes swell, forming bubble-like protrusions. Inside the cell, the nucleus disintegrates, and the chromatin (DNA and associated proteins) condenses, forming dense, compact structures. The cell then breaks apart into smaller, membrane-bound fragments known as apoptotic bodies. Finally, these apoptotic bodies are recognized and engulfed by phagocytic cells such as macrophages, ensuring the cell contents are retained and do not trigger an inflammatory response. This regulated process of cell lysis and removal is essential for normal development, immune system function, and cancer prevention.

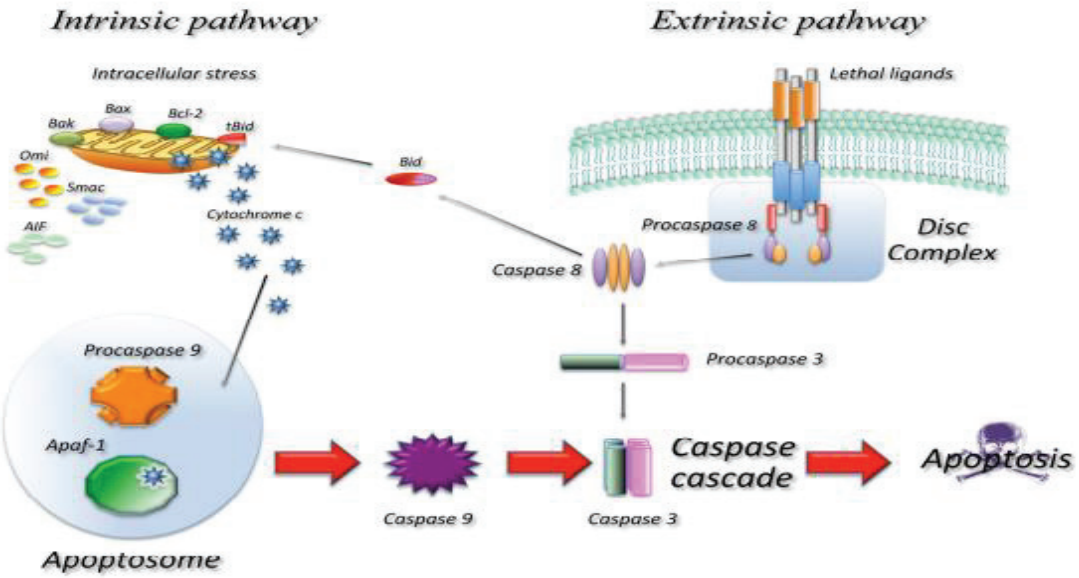

Figure 5. Extrinsic and Intrinsic Pathway of Apoptosis
(Source:Favaloro et al. 2012)

Apoptosis is distinguished by a range of unique morphological and biochemical alterations, such as membrane blebbing, DNA fragmentation, chromatin condensation, and shrinking of the cell. The intrinsic (mitochondrial) pathway and the extrinsic (death receptor) pathway are the two primary apoptotic pathways that mediate these modifications (Elmore 2007).

Intrinsic Pathway: Stress factors or damage to the cell's DNA initiate this process from inside. The process starts with a release of cytochrome c into the cytosol due to enhanced permeability of the outer membrane of the mitochondria. The apoptosome complex is created in the cytosol by the combination of cytochrome c and Apaf-1. Caspases 9 and 3 are activated by this combination, activating caspase-3. The cleavage of intracellular substrates by Caspase-3 causes the production of membrane blebs, nuclear fragmentation, chromatin condensation, and apoptotic bodies, which are the hallmarks of apoptosis. Ultimately, phagocytic cells remove these apoptotic bodies (Tait and Green 2010).

Extrinsic Pathway: This process is activated when extrinsic death ligands, such as TNF or FasL, attach to cell surface death receptors. The death-inducing signaling complex (DISC) is formed when death ligands bind to receptors. The DISC activates caspase-8. Caspases 3 and 8 are triggered by caspase-8. The cleavage of intracellular

substrates by Caspase-3 causes the production of membrane blebs, nuclear fragmentation, chromatin condensation, and apoptotic bodies, which are the hallmarks of apoptosis. Phagocytic cells remove these bodies (Ashkenazi and Dixit 1998).

1.5.2. Cell Cycle

Cell division, growth, and DNA replication are all part of the intricate and controlled cell cycle. The growth, repair, and homeostasis of organisms depend on this mechanism. The cell cycle consists of four main phases: the first growth phase (G1), the synthesis phase (S), the second growth phase (G2), and the mitotic phase (M). During the G1 phase, the cell grows and produces the necessary organelles. DNA replication occurs in the S phase, resulting in two copies of each chromosome. In the G2 phase, the cell ensures that DNA replication is complete and synthesizes the proteins required for mitosis. Finally, during the M phase, the cell undergoes mitosis and cytokinesis to divide into two new cells (Chaffey 2003) .

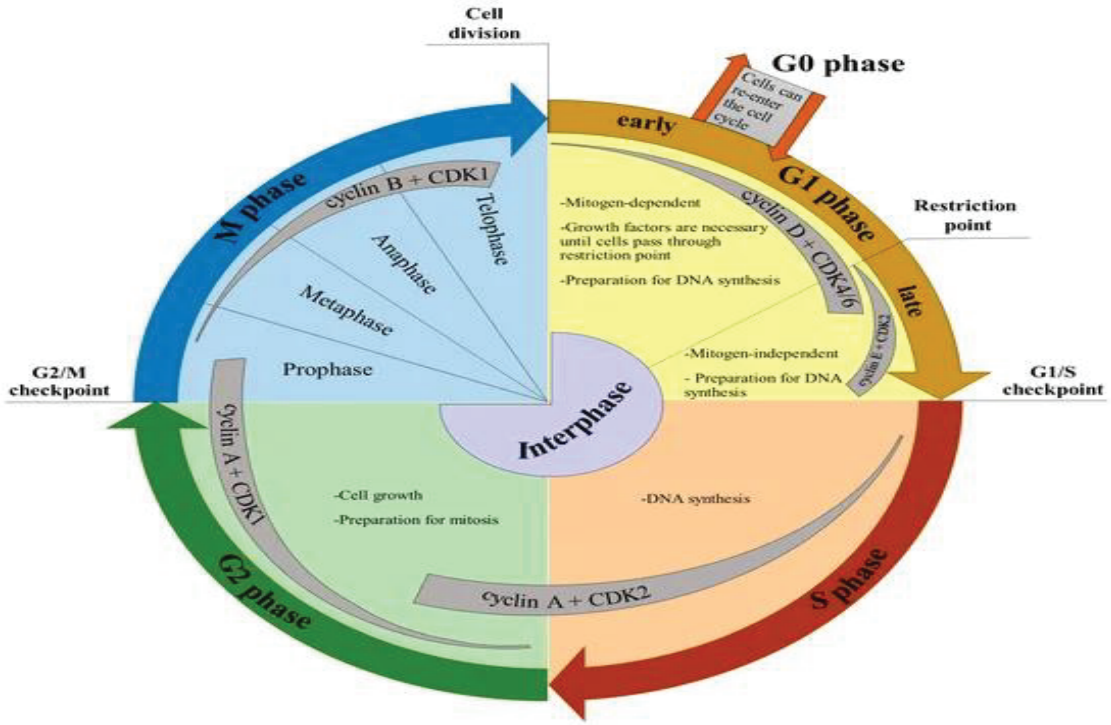

Figure 6. Cell Cycle Stages

(Source: Ligasová, Frydrych, and Koberna 2023)

Both external and internal signals carefully regulate the cell cycle. Proteins like cyclins and cyclin-dependent kinases (CDKs) facilitate this control. Cell cycle progression is regulated by activating cyclins and CDKs during specific cell cycle phases. For instance, the cyclin D-CDK4/6 complex pushes the cell cycle forward into the S phase during the G1 phase. The cyclin A-CDK2 complex starts DNA replication during the S phase. The cyclin B-CDK1 complex starts mitosis during the G2 phase (Lubischer 2007).

At specified periods in the cell cycle, the cell is examined to ensure it satisfies requirements before proceeding to the next stage. While the G2 checkpoint determines that DNA replication is finished and that no damage has occurred to the DNA, the G1 checkpoint confirms that the cell has grown to an appropriate size. The M checkpoint guarantees Chromosome separation during mitosis (Hartwell and Weinert 1989).

When the cell cycle operates properly, the organism's genetic integrity is preserved, and healthy cell division occurs. On the other hand, aberrant behavior in the control of the cell cycle can result in the emergence of several illnesses, including cancer. Cell division becomes uncontrollable in cancer due to a failure of cell cycle regulatory systems. Tumor development and the spread of cancer may result from this (Hanahan and Weinberg 2011).

Developing novel therapeutic approaches for cancer and other cell cycle-related disorders is made possible by understanding the molecular mechanisms underlying the cell cycle. For instance, targeted treatments that interrupt the cell cycle, like CDK inhibitors, stop cancer cells from multiplying (Sherr and Roberts 1999).

1.6. Serum protein binding

Serum protein binding is essential for controlling physiological and cellular functions. Serum contains proteins called albumin, globulins, and fibrinogen that help other molecules, including hormones and medicines, travel to target cells or tissues. These proteins are also crucial for coagulation, osmotic equilibrium, and immunological response. Specifically, albumin performs the transport function and binds to various ligands to maintain the blood plasma's osmotic pressure (Friedrichs 1997).

Serum protein binding affinity and capacity are crucial in pharmacokinetic and pharmacodynamic process determination. Drugs enter the bloodstream through binding

to serum proteins, which has an impact on the drugs' distribution, absorption, and disposal. For instance, medications with stronger albumin binding typically have longer half-lives and are biologically active for extended periods (Benet and Hoener 2002).

1.7. Hemolysis

Hemolysis is the breakdown and release of hemoglobin and other cellular components into the plasma by red blood cells, or erythrocytes. There are several physiological and pathological circumstances in which hemolysis may happen. Hemolysis releases free hemoglobin and other cellular components, which can cause kidney damage, oxidative stress in the circulatory system, and malfunction in other organs (Forget and Bunn 2013).

Hemolysis is also an important factor in drug delivery systems. Especially in nanoparticle-based drug delivery systems, hemolysis testing plays a critical role when evaluating the biocompatibility and toxicity profile of carriers. Nanoparticles provide effective delivery of drugs to targeted cells or tissues. However, the interaction of these carriers with red blood cells can lead to hemolysis, which may result in systemic toxicity and reduced treatment efficacy (Dobrovolskaia and McNeil 2013). Hemolysis analysis is a critical method for testing these nanosystems' safety and evaluating their potential toxicology.

CHAPTER 2

MATERIALS AND METHODS

2.1. Materials

All compounds have been obtained from Sigma unless specified otherwise.

2.1.1. Cell Lines

Two different human breast carcinoma cell lines, MCF-7 and MDA-MB-231, were obtained from Özden Yalçın Özuysal from İzmir Institute of Technology Department of Molecular Biology and Genetics.

2.1.2. Culture Media

Cell culture studies for MCF-7 and MDA-MB-231 cell lines were carried out with DMEM medium after adding 10% Fetal Bovine Serum (FBS), 1% Penicillin Streptomycin, and 1% L-glutamine. Since the medium alone is insufficient to create the necessary environment for cells, particular substances must be added. Fetal Bovine Serum (FBS) provides the fundamental nutritional source for cell growth and reproduction thanks to the vitamins, hormones, and minerals it contains. Penicillin is effective against gram-positive bacteria, and streptomycin is effective against gram-negative bacteria to prevent bacterial contamination. L-glutamine, an essential amino acid for cells, plays a role in energy production, protein synthesis, and cell proliferation.

2.1.3. Chemicals, Solutions, and Reagents

All chemicals have been obtained from Sigma unless stated otherwise.

2.2. Methods

2.2.1. Synthesis and optimization of ZIF-8 and MB@ZIF-8 nanoparticles

Firstly, small-sized ZIF-8 and MB@ZIF-8 nanoparticles were synthesized using the method developed by (Abdelhamid 2020) 200 mg of $Zn(NO3)_2.6H2O$ was weighed, transferred into a vial, and dissolved by adding 0.8 ml of pure water. 5.75 mg of 2-methylimidazole (2-MeIM) was dissolved in a separate vial in 23 mL of pure water. 64 mg of methylene blue (MB) was weighed in an eppendorf and dissolved with 1 ml of pure water, and added to the dissolved 2-MeIM solution. 2 ml of TEA (Triethylamine) solution was added to the $Zn(NO_3)_2.6H_2O$ solution and the mixtures were stirred at 1000 rpm overnight. 2-MeIM saturated solution was added dropwise into the $Zn(NO_3)_2.6H_2O$ solution. The cloudy blue solution formed is an indication that MB@ZIF-8 has been synthesized. The mixture was magnetically stirred for 15 minutes at room conditions and then centrifuged at 14,000 rpm for 15 minutes to precipitate the white MB@ZIF-8 solid. The remaining reactants were removed by washing the solution with ethanol three times and then dried at 65 ºC overnight to obtain ZIF-8 nanoparticles.

2.2.2. Nanoparticle Loading Efficiency

Using gravimetry analysis to establish the amount of weight of the nanoparticles produced by drying a known volume of nanoparticles, the yield of the synthesized nanoparticles was evaluated. The direct measurement was performed using inductively coupled plasma-optical emission spectrometry (ICP-OES) (Agilent 5110 Dual View, Agilent Technologies, United States) for dye-loading nanoparticle efficiency. After ICP-OES analysis, the particles were eluted in a 5% HNO3 aqueous solution before the measurement to determine the Zn composition of the whole particle material. The following formula was used to calculate the loading efficiency:

Loading efficiency (%) = (mass of dye in nano comp./mass of total loaded dye) × 100

The synthesis efficiency was 49,6%, while the loading capacity was calculated as 17,8%

2.2.3. Characterization of ZIF-8 and MB@ZIF-8 nanoparticles

Various analytical techniques will be employed to characterize the smart and functionalized nanoparticles. For this, scanning electron microscopy (SEM) analysis was used for imaging with a 5 KV electron beam and 200 nm scale using the equipment FEI QUANTA 250 FEG(USA) to investigate the nanoparticle surface area structure, the coating efficiency and the nanoparticles' size. The zeta potential of nanoparticles is a crucial element to remember, especially in vitro studies, in which the cellular retention rate is such a vital aspect. Consequently, the zeta potential and hydrodynamic radii of the prepared ZIF-8 and MB@ZIF-8 nanoparticles were evaluated with the Zetasizer Nano Z (Malvern Panalytical, UK) using the Dynamic Light Scattering Method (DLS). The extent of crystallization of nanoparticles was assessed using Powder X-ray Diffraction (XRD) with CuKα radiation in a Philips Xarakpert Pro diffractometer (Royal et al., The Netherlands) having a beam wavelength of 1.541 A and operating at 40 kV and 25 mA. Fourier Transform Infrared Analysis (FT-IR) (PerkinElmer, USA) was performed to identify the functional groups.

2.2.4. Thawing the Frozen Cells

Cells in a 2 mL cryotube frozen at -80°C were taken out of storage and allowed to thaw for two to three minutes in a water bath at 37°C. The cells were placed in a 15 mL sterile falcon after being diluted with around 4 mL of cell media. The DMSO was subsequently removed from the cell culture by centrifuging it for five minutes at 800 rpm at +4°C. Following centrifugation, the cells were resuspended in 5 mL of fresh cell media, the supernatant was thrown away, and the mixture was then put in a 25 cm^2 cell culture flask for proliferation. The cells were kept in an incubator with 5% CO_2 at 37°C.

2.2.5. Passaging the Cells

The biosafety cabinet (class II) was first UV sterilized for 15 minutes to prevent contamination. It was then cleaned with a 70% ethanol solution. Before getting put in the cabinet, each solution and medium used in cell passaging was cleaned individually with

a 70% ethanol solution after being heated in a 37°C water bath. For passaging, cells with 80% growth were removed from the incubator. The 75cm^2 cell flask's old medium was removed and carefully cleaned multiple times using 9 mL of sterile PBS (3 mL per 25cm^2 surface area). After removing the PBS, 3 mL of trypsin (1 mL per 25cm^2 surface area) was added to activate the cells and separate them from the flask surface. The cells were then incubated for 5 minutes at 37°C with 5% CO_2. 9 mL of fresh media (3 mL per 25cm^2 surface area) was added once it was confirmed that every cell had been lifted from the surface, and it was then gently rinsed multiple times. After that, the cell suspension was put into a 15 mL sterile falcon and centrifuged for 5 minutes at 800 rpm. Centrifugation was used to extract the supernatant. Centrifugation was used to extract the supernatant. Depending on the type and density of the cells, the cell pellet was resuspended in fresh media, and 1 mL was transferred to a fresh cell flask with enough fresh cell medium in it. After that, the cells were incubated with 5% CO_2 and 37°C to grow.

2.2.6. Freezing the Cells

Following cell passaging, the cell pellet was resuspended in 15 mL of falcon with fresh cell media. Then, 10% FBS and 10% dimethyl sulfoxide (DMSO) were gently pipetted into the homogenized volume and transferred to 2 mL cryotubes. Cell continuity and storage were provided by keeping the cells in the cryotubes at -80°C.

2.2.7. Counting the Cells

After resuspending the cell pellet with fresh media in the falcon, 100 µL of cells were removed and placed in a 1.5 mL eppendorf. The cell culture was well mixed with 100 µL of 0.4% trypan blue solution using the up-down method. Carefully placed on the hemocytometer, a little portion of the mixed suspension was taken for counting. Under a microscope, viable cells that seemed opaque in the hemocytometer squares were counted. The number of cells in one milliliter was determined using the formula below.

$$\text{Number of cells per mL} = (\text{average counted of cell number})^2 \times \text{dilution factor} \times 10^4 \quad (2.1)$$

2.2.8. Cell Viability Assay (MTT Test)

The MTT assay evaluated the cytotoxicity of newly synthesized ZIF-8 and MB@ZIF-8 derivatives. MCF-7 and MDA-MB-231 cells at a density of 25×10^3 were seeded in 96-well plates with a growth area of 95 µL per well and incubated at 37 °C in 5% CO_2 for 24 hours. Compounds were dissolved in sterile DMSO and diluted as needed with culture medium (300–150–75–60–30–15 µg). The final DMSO concentration had been modified to 1% in each well. After a 24-hour incubation period, the cells were removed from the incubator, and 5 µl of the suitable nanoparticle concentration was added to each 96-well plate well. Cells treated with nanoparticles were incubated for 12 and 24 hours to determine the cytotoxic effects. At the end of each incubation period, 10 µL of MTT dye solution (5 mg/mL PBS) was applied to each well in order to reduce the amount of tetrazolium salt. After that, the wells were kept at 37°C in an incubator with 5% CO_2. After the 96-well plate was incubated for 3.5 hours, the supernatant was removed by centrifuging the plate for 10 minutes at 1800 rpm. Following the addition of 100 µL of DMSO to dissolve the formazan crystals, each well was shaken up for 15 minutes to ensure homogeneity. At 540 nm, optical density was determined using Variscan Flash.

2.2.9. Reactive Oxygen Species (ROS) Detection Assay

The ROS production capacity of the synthesized nanocarrier system was measured in the cell. For these measurements, Rhodamine 123 was supplied by Assoc. Professor Dr. Muhammed ÜÇÜNCÜ Katip Çelebi University. ZIF-8 and MB@ZIF-8 were added to cells at concentrations based on IC50 values and PDT with ideal time trials (30 min, one hour), and the cells were subsequently incubated for 24 and 48 hours. Each well received an addition of 0.1 mL of ROS detection solution. A fluorogenic sensor in the solution reacts with ROS to produce a fluorometric product proportionate to the ROS concentration. After giving the cells another 30-minute incubation period, the fluorescence was eventually found using a fluorescent multiwall plate reader set to detect emission wavelengths and excitation of 520 and 490 nm, respectively.

2.2.10. Apoptosis Analysis

Using the Annexin V-FITC kit methodology, the PDT-induced cell death patterns initiated by ZIF-8 and MB@ZIF-8 were examined. Cell lines were incubated in 1980 µL for 24 hours in 6-well plates containing $25x10^3$ cells per well. After being dissolved in sterile DMSO, ZIF-8 and MB@ZIF-8 were added to the cells in 20 µL at the proper doses. Following a 24-hour CO_2 incubation period at 37°C, cells were collected along with their medium and placed into 15 mL falcons. Subsequently, 1 mL of phosphate-buffered saline (PBS) was used to wash each well. Trypsin (250 µL) was added to raise the cells, and each cell was collected in its falcon. For five minutes, the collected cells were centrifuged at 800 rpm. Repeated washing and centrifuging were performed after dissolving the precipitate in PBS. 200 µL of the binding kit buffer was used to suspend the final precipitate, and then 2 µL of the Annexin V-FITC dye and 5 µL of propidium iodide dyes were added. After a 15-minute incubation period, the solution was measured using a Flow Cytometry device.

2.2.11. Cell Cycle Analysis

MCF-7 and MDA-MB-231 cells were incubated in 6-well plates with 25×10^3 cells per well in 1980 µL of medium at 37 °C with 5% CO_2 for 24 hours. ZIF-8 and MB@ZIF-8 were dissolved in sterile DMSO and added to the cells at appropriate concentrations. After 24 hours, cells were harvested using 250 µL of trypsin, then centrifuged at 800 rpm for 5 minutes. The supernatant was discarded, and the pellet was resuspended. To fix the cells, 1 mL of cold PBS and 4 mL of -20 °C ethanol were added, and the mixture was incubated at -20 °C for at least 24 hours. The tubes were centrifuged at 1200 rpm for 10 minutes to remove the ethanol and PBS. The pellet was resuspended in 5 mL of PBS and centrifuged again at 1200 rpm for 10 minutes. After carefully removing the supernatant, 20 µL of RNase A (200 µg/mL) and 200 µL of 0.1% Triton X-100 in PBS were added. The cell suspensions were incubated at 37 °C for 30 minutes. Flow cytometry analysis was performed using a BD FACSCanto.

2.2.12. Serum Protein Binding and Hemolysis Analysis

Fetal bovine serum (FBS): nanoparticle mixtures with final volumes of 1000 µL were generated at ratios of 10:90, 20:80, 30:70, 50:50, 70:30, 80:20, and 90:10 (v/v). After two hours of incubation at 37 °C, the mixtures were centrifuged. Pellets were cleaned using a pH 7.4 PBS buffer. Protein in supernatants was determined using the Bradford 46 assay (Bradford 1976), after which the amount and yield of protein binding were calculated.

Erythrocytes were incubated at 37°C for four hours, with concentrations of 25, 50, 75 and 100 µg/mL of produced ZIF-8 and MB@ZIF-8 nanoparticles mixed with PBS solution at a 1:1 (v/v) ratio, in order to measure the hemolysis potential. One positive control group was treated to 1% Triton X-100 and the other to PBS. Centrifugation was used to extract the mixture's nanocarriers and erythrocytes after the incubation. Samples from the supernatant were obtained at 540 nm and analyzed spectrophotometrically for hemoglobin measurement. The hemolysis rate was computed using the following formula for absorbance (Mayer et al. 2009).

(% Hemolysis = (A sample - A negative control) * 100/A positive control) (2.2)

2.2.13. Dye Release Studies

Release experiments were performed at pH 5.5 and physiological pH 7.4, which are similar to the tumor cell environment. PBS was used to test 6 mg ZIF-8 and MB@ZIF-8 nano delivery systems in 2 mL at physiological temperature (37°C), pH = 7.4 and 5.0, and constant shaking. New PBS was added every time the centrifuged supernatant was extracted, and PBS samples were taken between 0 and 80 hours. Supernatants' absorbance was measured using a UV-Vis spectrophotometer (Shimadzu-UV-2550 Japan). The amount of released dye was calculated using the dye's maximal absorbance peak as a guide. (At 635 nm for Methylene Blue)

CHAPTER 3

RESULTS AND DISCUSSION

3.1. Characterization

3.1.1. Fourier Transform Infrared Analysis (FT-IR)

Functional groups present in ZIF-8 and MB@ZIF-8 were determined by Fourier Transform Infrared Analysis (FT-IR) (PerkinElmer, ABD) (Figure 7). The bands at 3135 and 2928 cm^{-1} in the ZIF-8 spectrum represent the aromatic C–H stretching and aliphatic C–H stretching of imidazole. The 1606 cm^{-1} band is for the C–C stretching vibration, and the peak at 1580 cm^{-1} represents the C–N stretching. The C–N absorption bands are located in the 1100–1400 cm^{-1} region. The absorption band at 1421 cm^{-1} is associated with the Zn–N stretching mode. In the pure FTIR spectrum of MB (Methylene Blue), NH/-OH shows a prominent band for overlapping stretching vibration, which is located at 3360 cm^{-1}. The correlations of absorption peaks belonging to other functional groups associated with MB are as follows: C=C side ring stretching at 1497 cm^{-1}, CH=N at 1605 cm^{-1}, $-CH_2$ or $-CH_3$ stretching at 1377 cm^{-1}, -C-N and N-N stretching absorption peaks are located at 1252 cm^{-1} and 1215 cm^{-1} respectively. Other MB absorption peaks include C-N at 1137 cm^{-1} C-S-C at 1046 cm^{-1} and C-H bending vibrations outside the ring at 830 cm^{-1}. The FTIR spectrum for the MB@ZIF-8 system is similar to that of ZIF-8. This result is associated with the encapsulation of MB into ZIF-8 and the absence of adsorption.

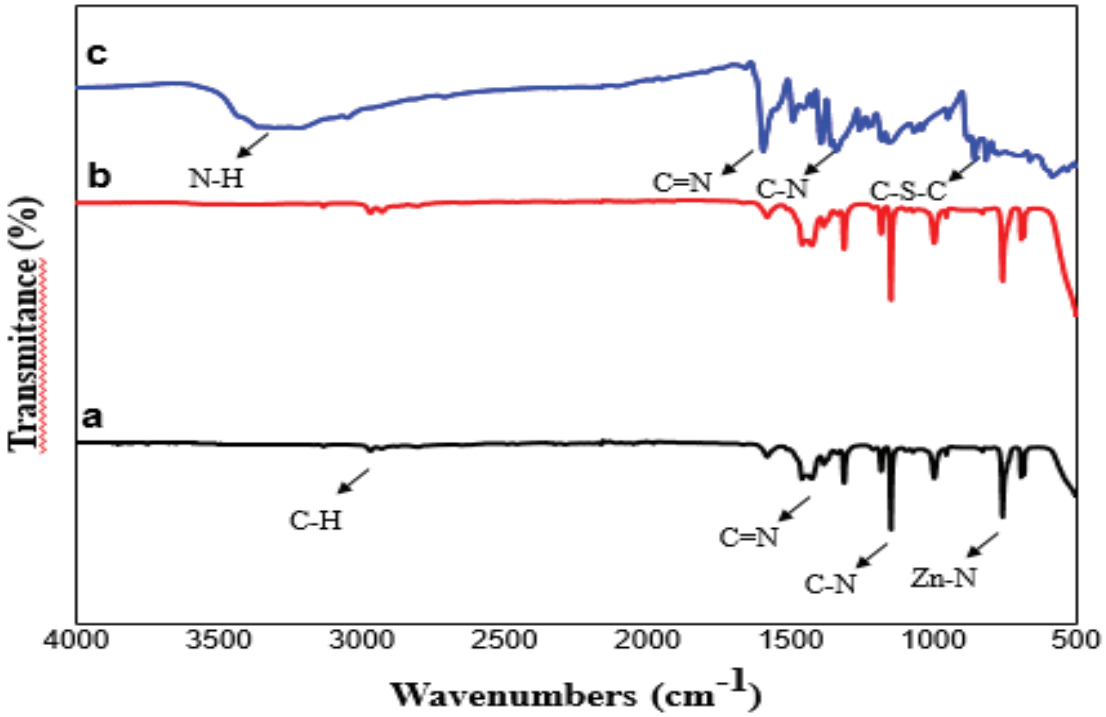

Figure 7. FTIR spectra for a) ZIF-8 b) MB@ZIF-8, and c) MB

3.1.2. Powder X-ray Diffraction (PXRD)

The crystallinity of the nanoparticles produced due to the synthesis of ZIF-8 and MB@ZIF-8 nanoparticles was examined using PXRD analysis. CuKα radiation was used for XRD analysis using a Philips Xarakpert Pro diffractometer (Royal et al., The Netherlands), which was kept at 40 kV and 25 mA and had a beam length of 1.541 Å. Diffractograms showing the diffraction patterns of the nanoparticles are shown in Figure 8. PXRD analysis results showed that 2θ= 7.34°, 10.46°, 12.79°, 14.75°, 16.53°, 18.12°, 22.21°, 24.56°, 26.77°, 29.76°, 30.67°, 31.62°, 32.46° peaks were observed for ZIF-8 and MB@ZIF-8 nanoparticles. These peaks overlap with the characteristic (011), (002), (112), (022), (013), (222), (114), (233), (134), (044), (334), (244), (235) indices of ZIF-8 known in the literature, respectively, and verify the sodalite structure, which is ZIF-8's characteristic structure. This result shows that the crystalline ZIF-8 and MB@ZIF-8 nanoparticles were successfully synthesized. The patterns produced by the ordered porous structure of the peak broadening of the ZIF-8 particles indicated the formation of nano-sized crystals. MB shows an amorphous PXRD pattern. In addition, the fact that the diffraction pattern of MB@ZIF-8 is identical to ZIF-8 suggests that the MB dye may be

present in the cavities in the ZIF-8 nanoparticles instead of forming any complex in the reaction medium. At the same time, the octahedra crystallinity of ZIF-8 is preserved.

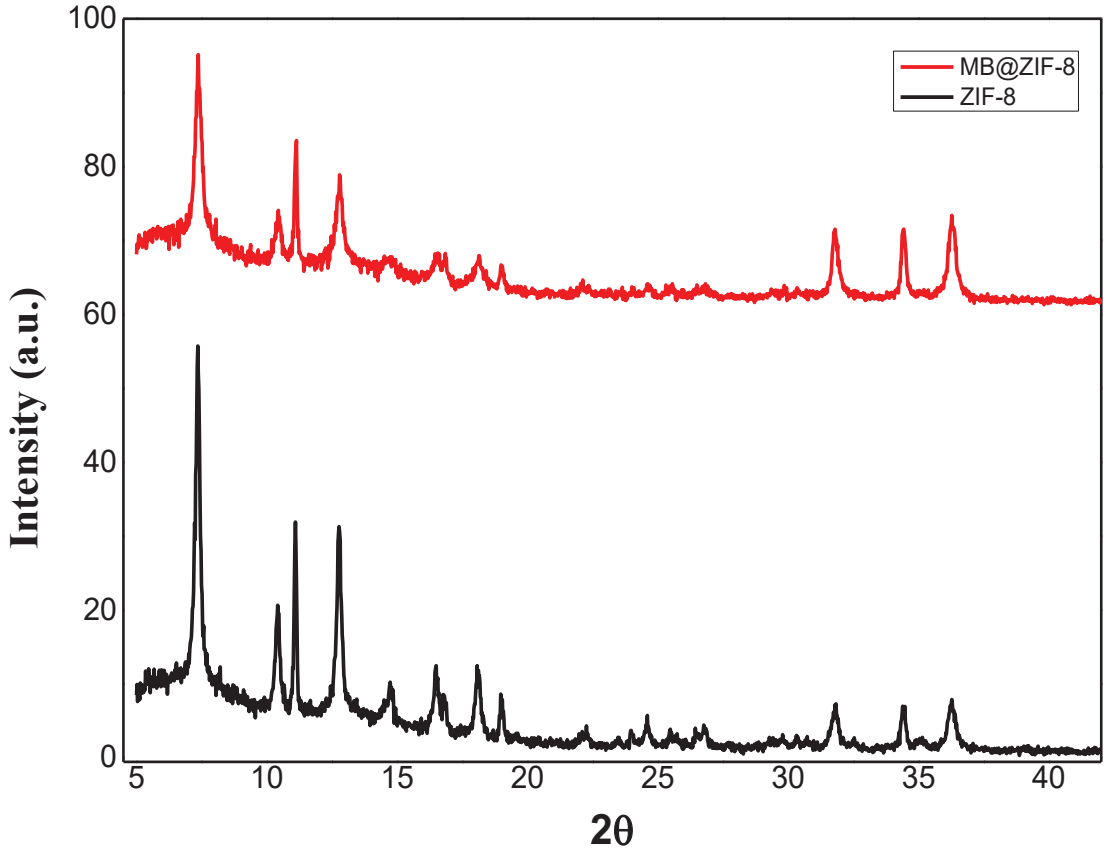

Figure 8. XRD patterns of a)ZIF-8 and b)MB@ZIF-8

3.1.3. Scanning Electron Microscopy (SEM)

SEM analyses were performed to evaluate the samples' surface morphology, porosity, and layer thickness using an FEI QUANTA 250 FEG (USA) device with a 5 kV electron beam and a 200 nm scale. The SEM images revealed that the samples consisted of homogeneously distributed rhombic dodecahedral-shaped nanoparticles. The particle size was calculated to be 124.9 nm for ZIF-8 and 150.1 nm for ZIF-8@MB. These findings align with the study by (Kaur et al. 2017) where ZIF-8 nanoparticles were observed with a hexagonal shape—a typical morphology for ZIF-8—and particle sizes ranging from 80 to 200 nm. Furthermore, the Dynamic Light Scattering (DLS) analysis conducted in this study also demonstrated an increase in particle size as more dye was loaded, consistent with the SEM results.

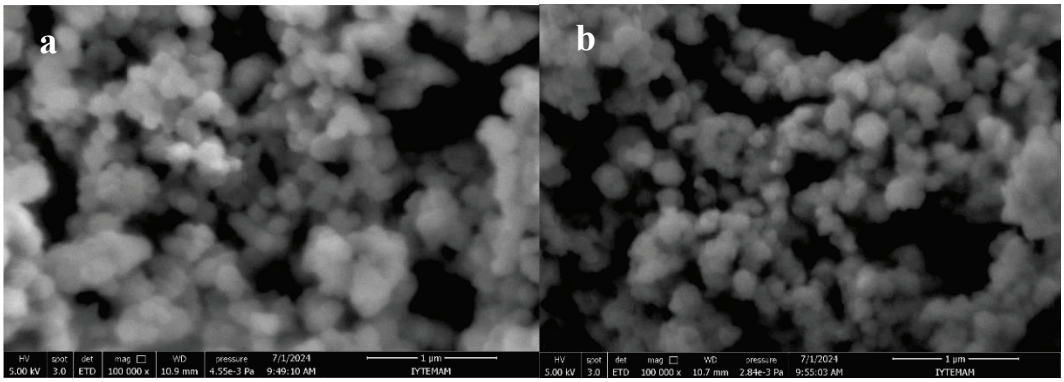

Figure 9. SEM micrographs of a)ZIF-8 and b) MB@ZIF-8

3.1.4. Dynamic Light Scattering Method (DLS) and Zeta Potential

Dynamic light scattering (DLS) was employed to explore particle size characteristics. The produced nanoparticles were dispersed in ethanol to achieve a stable suspension. The average hydrodynamic radius of ZIF-8 was measured at approximately 387.2 nm. Upon loading with methylene blue (MB), this radius appeared to increase to around 769.7 nm. This observed increase in particle size might be attributed to the MB loading, suggesting that the presence of the dye could be influencing the expansion of the ZIF-8 particles.

The polydispersity index (PDI) is a measure of the distribution of particle sizes within a sample, where a lower PDI indicates a more uniform size distribution and a higher PDI suggests more significant variability in particle sizes. In this study, the PDI value for ZIF-8 was found to be 0.355, indicating a relatively narrow size distribution and uniform particle size. For MB@ZIF-8, the PDI was even lower at 0.296, suggesting an even more uniform size distribution after loading methylene blue (MB) onto ZIF-8. This decrease in PDI after dye loading indicates that the process led to a more homogeneous nanoparticle population, possibly due to the stabilization effect of MB on the ZIF-8 framework, resulting in reduced variability in particle sizes. These results suggest that the dye loading process did not disrupt the size uniformity of the ZIF-8 particles but instead enhanced it.

The zeta potential of MB@ZIF-8 was measured at 35.51 mV, higher than the 24.5 mV of ZIF-8. This increase in zeta potential may indicate that the surface charges of ZIF-

8 particles are enhanced after loading with MB dye, potentially leading to greater electrostatic repulsion and improved stability. Particles with zeta potentials between 20 to 40 mV are typically considered moderately stable, suggesting that MB dye loading could have contributed to increased stability in the ZIF-8 particles.

Table 3.1 Hydrodynamic Radius and Zeta Potential of ZIF-8 and MB@ZIF-8

	Hydrodynamic Radius (nm)	**Zeta Potential (mV)**
ZIF-8	387.2	24.5
MB@ZIF-8	769.7	35.51

3.2. IC50 Values

As shown in Table 3.2, the IC50 values at all concentrations have been determined. According to the MTT assay results, the cell viability for MDA-MB-231 cells was 176.5 for ZIF-8 and 126.5 for MB@ZIF-8 under dark conditions. When these cells were incubated for 24 hours, followed by a 1-hour exposure to 40 mW red light, the cell viability decreased to 101.2 for ZIF-8 and 62.42 for MB@ZIF-8. Similarly, for MCF-7 cells, the cell viability under dark conditions was 183.1 for ZIF-8 and 147.9 for MB@ZIF-8, while after 24 hours of incubation and 1-hour red light exposure, these values dropped to 131.9 and 84.81, respectively. The IC50 concentrations inhibited 50% of the cells at each incubation time and were calculated using GraphPad Prism 10 (GraphPad Software and Inc.,USA). These results demonstrate the effectiveness of red light exposure in enhancing cell death.

Table 3.2 IC50 Values of MDA-MB-231 and MCF-7 cell lines at different concentrations

MDA-MB-231	**ZIF-8**	**MB@ZIF-8**
24h Dark	176.5	126.5
24h inc one h 40mw red light	101.2	62.42
24h inc 30min 40mw red light	95.12	75.39
12h inc one h 40mw red light	75.19	62.81

(cont. on next page)

Table 3.2 (cont.).

MCF-7	ZIF-8	MB@ZIF-8
24h Dark	183.1	147.9
24h inc one h 40mw red light	131.9	84.81
24h inc 30min 40mw red light	108.5	95.05
12h inc one h 40mw red light	98.46	83.33

3.3. Cell Viability Assay

The effects of the synthesized ZIF-8 and MB@ZIF-8 nanoparticles applied at concentrations of 300-150-75-60-30-15 µg/mL in the dark on cell viability in MDA-MB-231 and MCF7 cell lines were investigated using the MTT test (Figure 10-11). According to the MTT data obtained, it was observed that the nanoparticles caused toxicity in MCF-7 and MDA-MB-231 cells at concentrations of 150 and 300 µg/mL in the dark. In dark environment experiments with the MFC-7 cell line at a concentration of 75 µg/mL and following a 24-hour incubation period, the cell viability was determined to be 76% and 68% for ZIF-8 and MB@ZIF-8 nanoparticles, respectively. For the MDA-MB-231 cell line, cell viability was observed to be 70% and 61% for ZIF-8 and MB@ZIF-8 nanoparticles, respectively. No significant cytotoxic effect was observed for either cell line at concentrations below 75 µg/mL.

Figures 11 and 12 show the effects of synthesized ZIF-8 and MB@ZIF-8 nanoparticles at concentrations of 300, 150, 75, 60, 30, and 15 µg/mL on the cell viability of MDA-MB-231 and MCF-7 cell lines after a 24-hour incubation period, followed by a 60-minute exposure to red light at a power of 40 mW/cm², as determined by the MTT assay results. Upon light application to the MDA-MB-231 cell line, MB@ZIF-8 nanoparticles induced approximately 16.3% greater cellular inhibition on average compared to ZIF-8 at concentrations of 15, 30, 60, and 75 µg/mL. No significant difference was observed at 150 and 300 µg/mL due to toxicity. For the MCF-7 cell line, no significant difference was seen at 15 and 30 µg/mL, but MB@ZIF-8 showed better efficacy at concentrations of 60 µg/mL and above. When activated by light, MB generates reactive oxygen species (ROS), leading to oxidative stress and cell death. Hence, MB@ZIF-8 exhibited higher toxicity compared to ZIF-8 in both cell lines. With a 24-

hour incubation and 1-hour exposure to 40 mW/cm² red light, cell viability for 60 µg/mL MB@ZIF-8 was found to be 47% in the MDA-MB-231 cell line, compared to 58% in the MCF-7 cell line under the same conditions. When examining the other data obtained, it appears that the MDA-MB-231 cell line tends to exhibit lower viability rates compared to the MCF-7 cell line.

Due to the toxicity observed at 150 and 300 µg/mL in the dark, ZIF-8 and MB@ZIF-8 nanoparticles were applied to MDA-MB-231 and MCF-7 cell lines at 15, 30, and 60 µg/mL concentrations. Subsequent light application and incubation experiments were conducted at these concentrations.

After 12 hours of incubation, cellular viability for MB@ZIF-8 nanoparticles in the MDA-MB-231 cell line was 51% at 60 µg/mL and 61% in the MCF-7 cell line following 60 minutes of 40 mW/cm² red light application (Figure 14-15). After 24 hours of incubation, cellular viability was 58% for the MDA-MB-231 cell line and 65% for the MCF-7 cell line under the same nanoparticle concentration but with 30 minutes of red light application at the same power (Figure 16-17). These results suggest that lower cell viability is associated with 60 minutes of light exposure after 12 hours of incubation. Additionally, the MDA-MB-231 cell line consistently showed lower viability under both conditions. The results suggest that extending the light exposure time, which allows for more prolonged activation of the photosensitizer, may lead to increased cell death due to more reactive oxygen species (ROS) production.

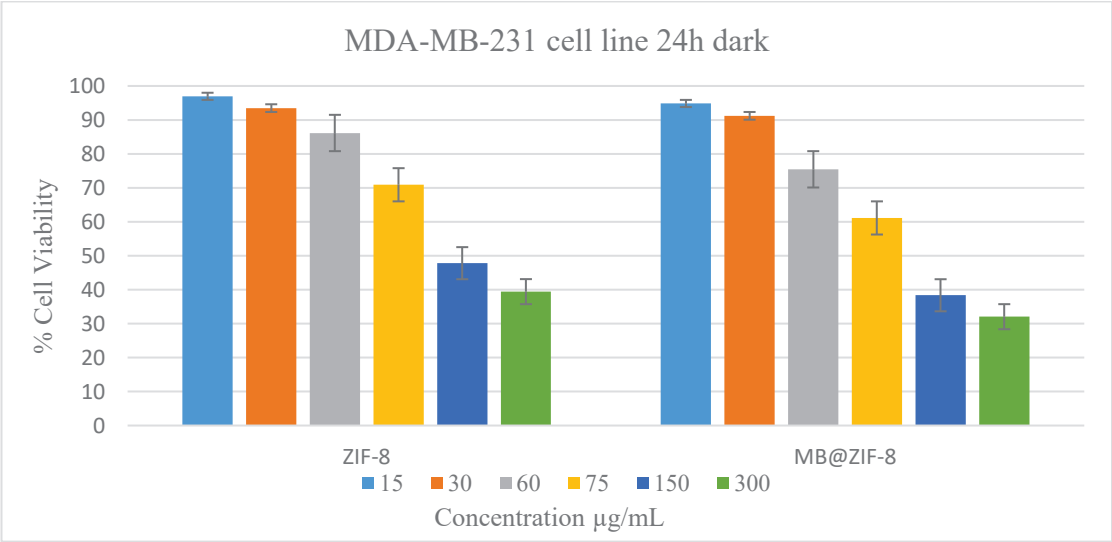

Figure 10. Effect of nanoparticles applied in the dark after 24 hours on MDA-MB-231cell lines.

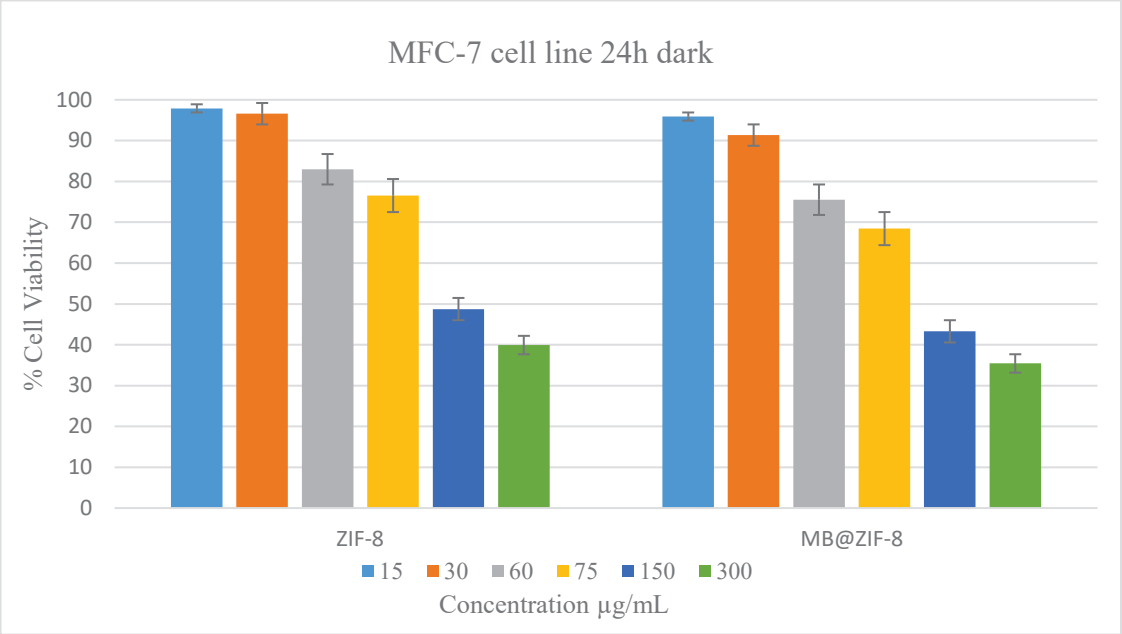

Figure 11. Effect of nanoparticles applied in the dark after 24 hours on MCF7 cell lines.

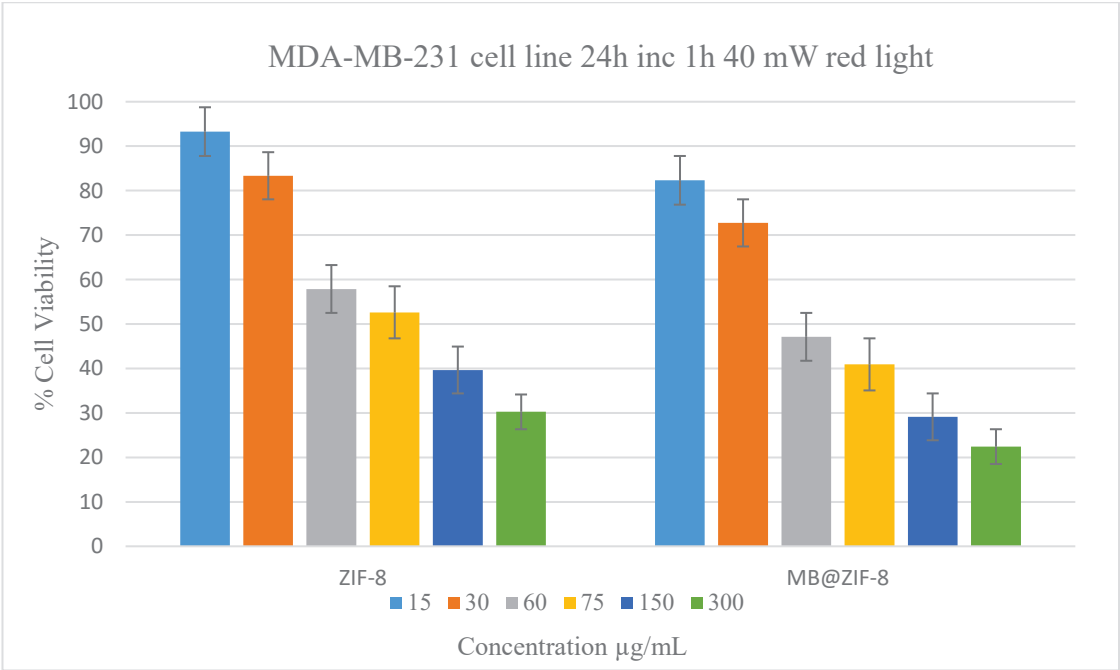

Figure 12. Effect of 60 minutes of application of 40 mW/cm^2 red light on MDA-MB-231 cell lines after 24 hours nanoparticles applied

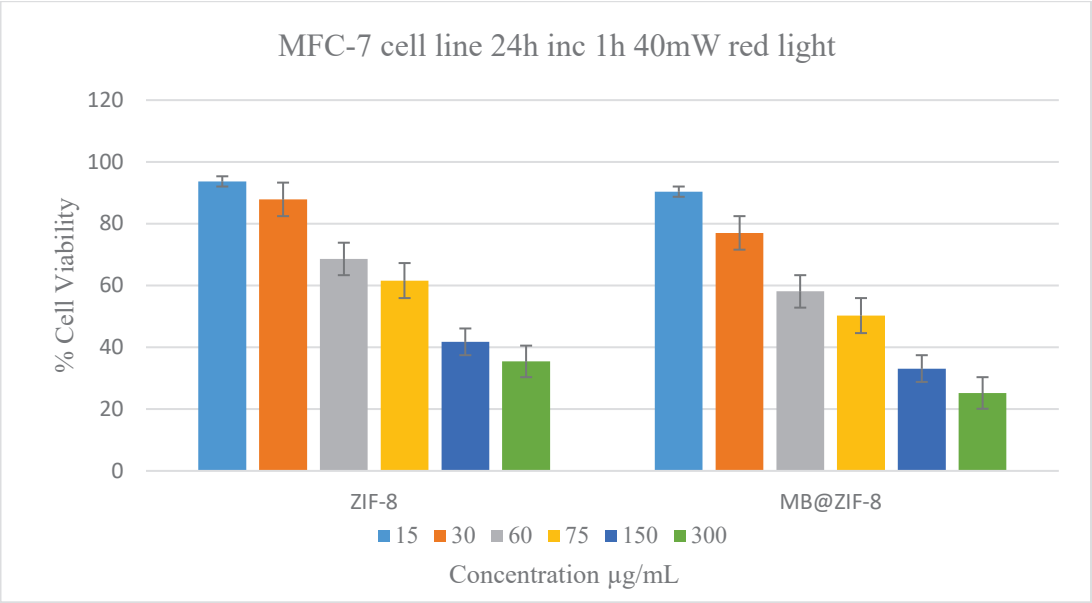

Figure 13. Effect of 60 minutes of application of 40 mW/cm^2 red light on MCF-7 cell lines after 24 hours nanoparticles applied

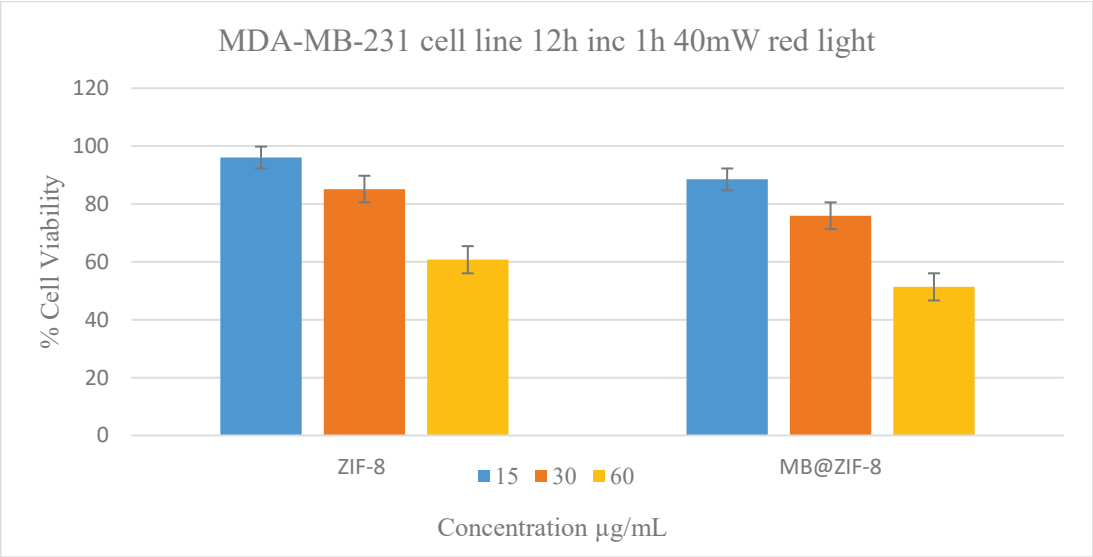

Figure 14. Effect of 60 minutes of application of 40 mW/cm^2 red light on MDA-MB-231 cell lines after 12 hours nanoparticles applied

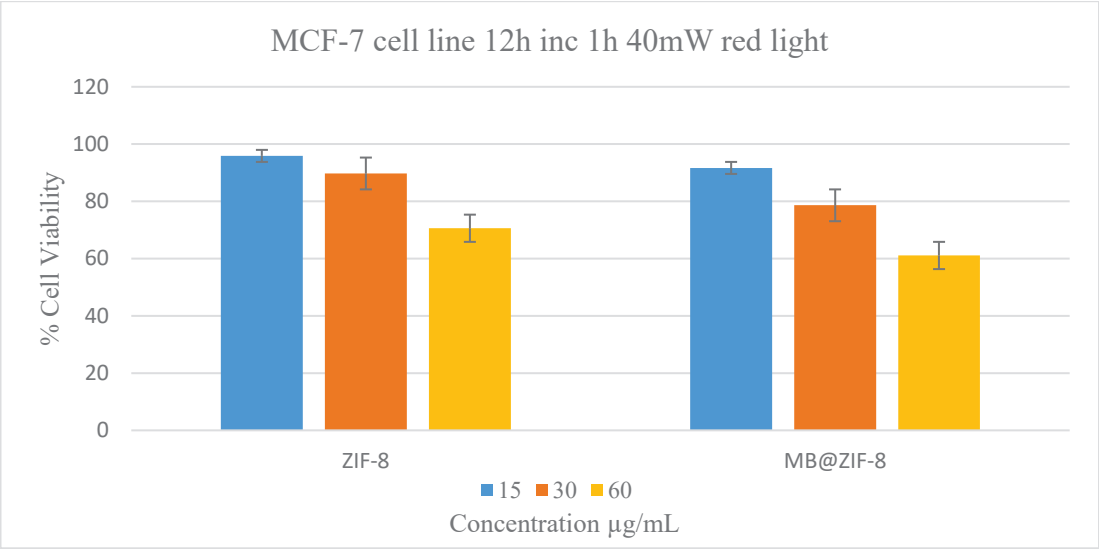

Figure 15. Effect of 60 minutes of application of 40 mW/cm^2 red light on MCF-7 cell lines after 12 hours nanoparticles applied

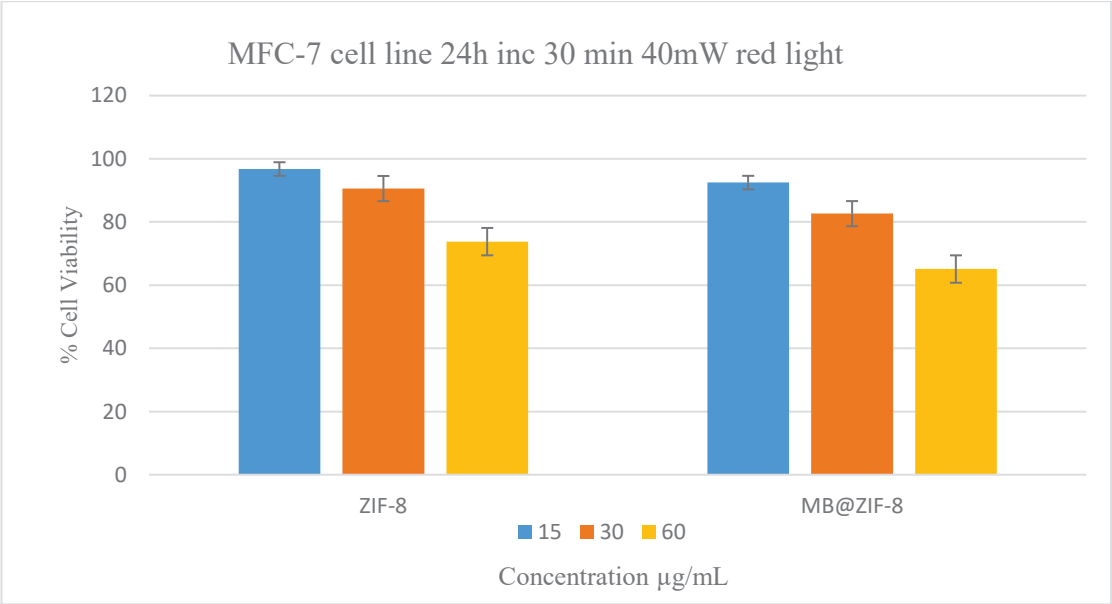

Figure 16. Effect of 30 minutes of application of 40 mW/cm^2 red light on MFC-7 cell lines after 24 hours nanoparticles applied

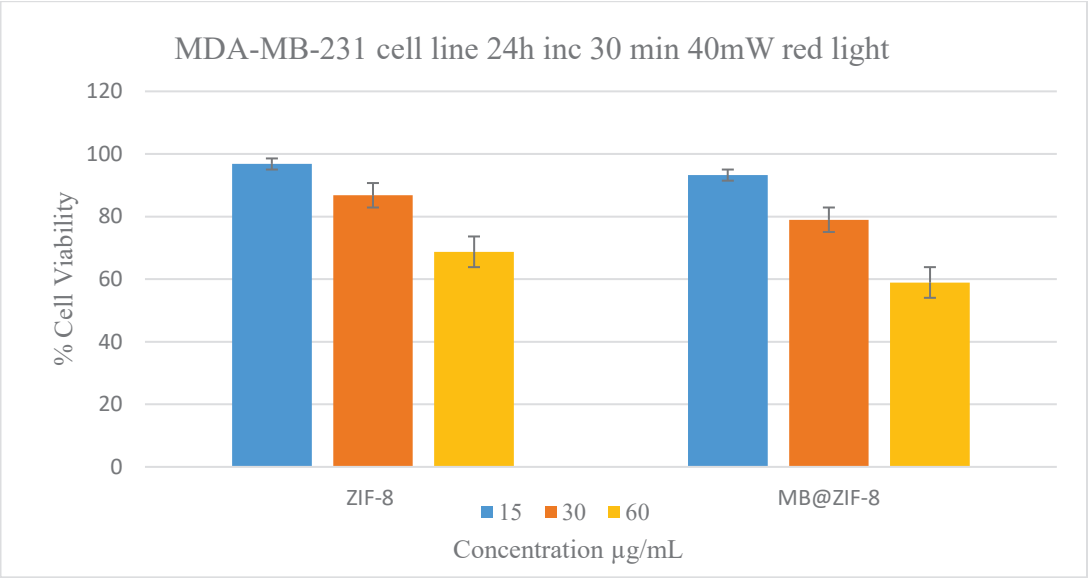

Figure 17. Effect of 30 minutes of application of 40 mW/cm^2 red light on MDA-MB-231 cell lines after 24 hours nanoparticles applied

3.4. Reactive Oxygen Species (ROS) Detection Assay

Figures 18 and 19 illustrate the ROS release in MDA-MB-231 and MCF7 cell lines following 24 hours with 60 minutes of exposure to 40 mW/cm² red light. As the concentration increased, the ROS level increased significantly. Furthermore, MDA-MB-231 cells demonstrated a higher release of ROS level relative to MCF7 cells.

According to the ROS results obtained using Rhodamine 123 dye, ZIF-8 alone was observed to trigger the lowest ROS levels. In contrast, its incorporation into the Methylene Blue ZIF-8 complex resulted in higher ROS levels. A possible explanation for this could be that cells treated with ZIF-8 experience excessive zinc accumulation, which may elevate ROS levels and contribute to cellular inflammation. The slow and controlled release of the dye by ZIF-8, combined with the regeneration potential of Zn^{2+} ions released during ZIF-8 degradation, is likely to enhance oxidative stress and subsequently increase the production of reactive oxygen species (ROS).

In the MDA-MB-231 cell line, a significant increase in ROS levels (2277.55 RFU) was observed at a concentration of 300 µg/ml. Elevated ROS levels were also noted at other concentrations, suggesting that MDA-MB-231 cells exhibit a pronounced oxidative stress response to MB@ZIF-8. In contrast, the MCF-7 cell line displayed much lower ROS levels in response to MB@ZIF-8, with ROS levels not exceeding 133.51 RFU even

at a concentration of 150 µg/mL. This suggests that MCF-7 cells may exhibit a weaker oxidative stress response to MB@ZIF-8.

Figure 20 illustrates the change in ROS levels in the MDA-MB-231 cell line after 24-hour incubation, followed by 1 hour of 40 mW/cm² red light exposure, 1 hour in the dark, and another hour of light exposure.

Figure 21 shows the change in ROS levels after 24 hours of incubation, 1 hour of 40 mW/cm² red light exposure, followed by a dark period, and another hour of light exposure at the end of 48 hours. In both experiments, ROS levels were observed to increase by 4.5 times. However, the anticipated high ROS production during the extended dark period (48 hours) with MB@ZIF-8 nanoparticles was not observed. The higher ROS production observed after the shorter dark period (1 hour) might be attributed to the cells' repair mechanisms being more active during this waiting period.

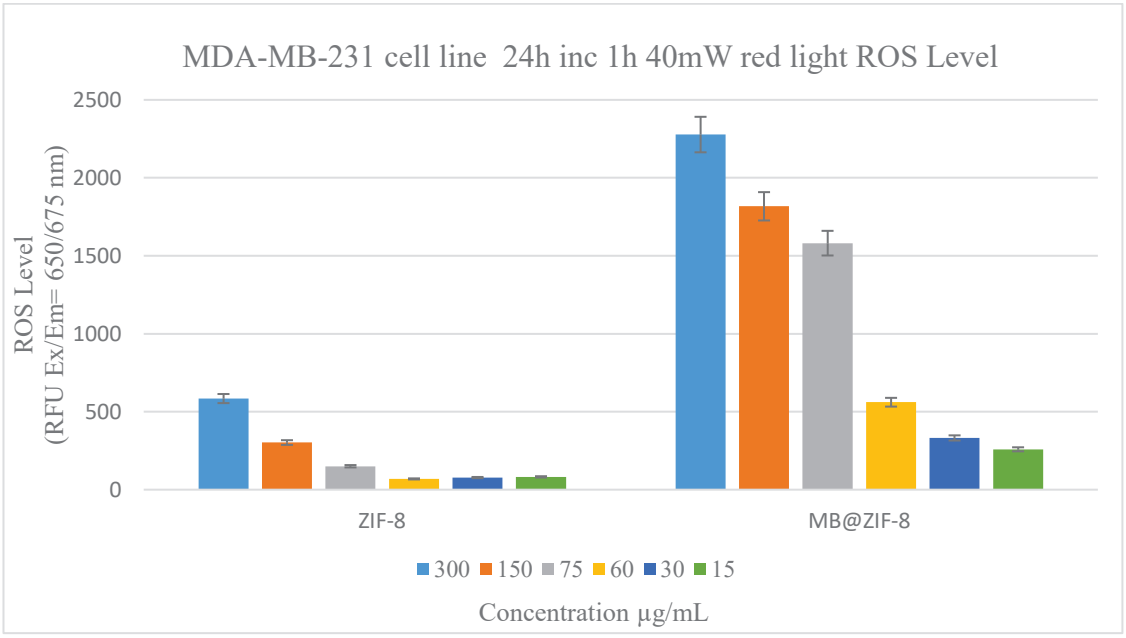

Figure 18. Effect of 60 minutes of application of 40 mW/cm^2 red light on MDA-MB-231 cell lines after 24 hours nanoparticles applied ROS level

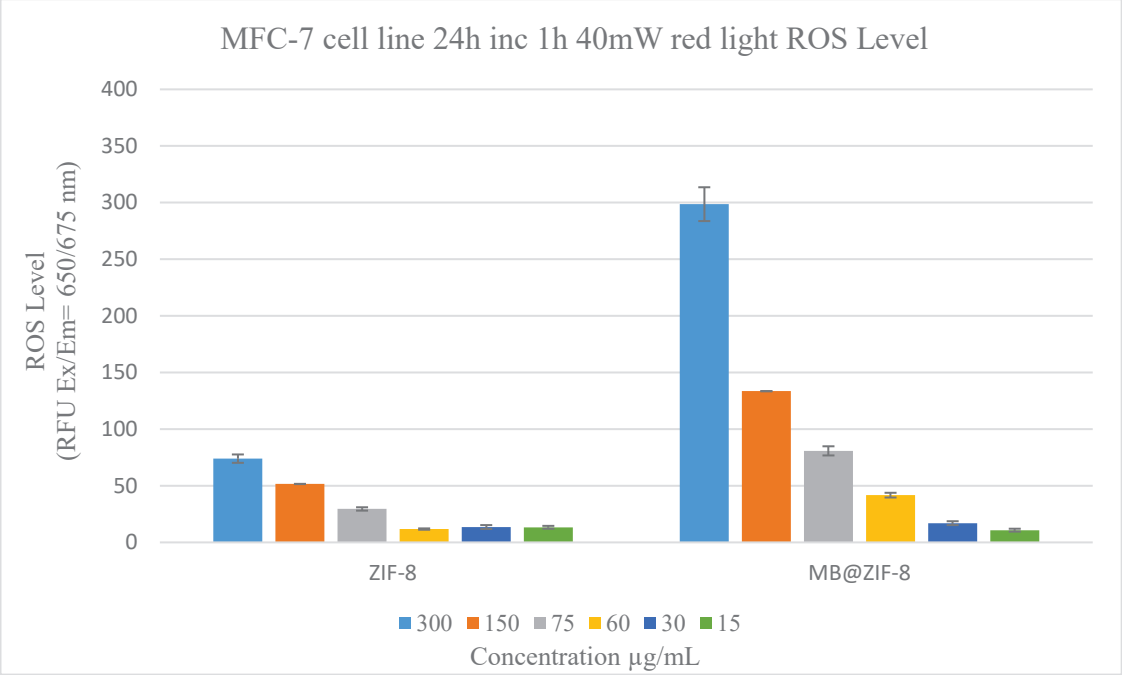

Figure 19. Effect of 60 minutes of application of 40 mW/cm^2 red light on MCF-7 cell lines after 24 hours nanoparticles applied ROS Level

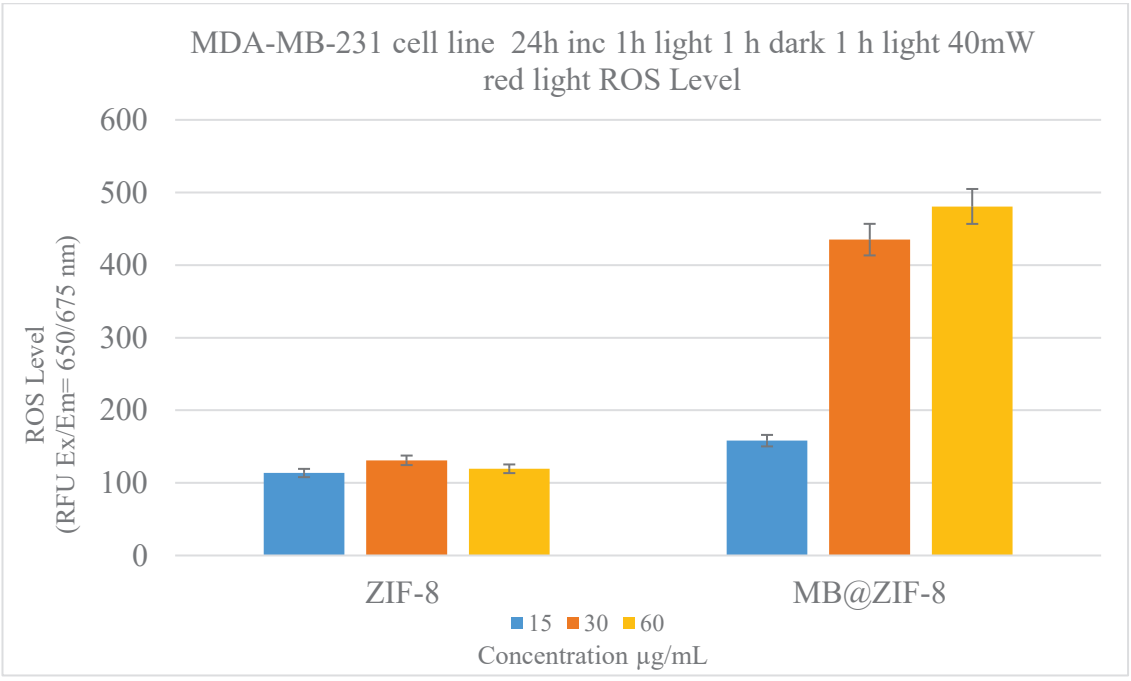

Figure 20. Effect of 60 minutes of application of 40 mW/cm^2 red light, 60 minutes dark, then 60 minutes red light application again on MDA-MB-231 cell lines after 24 hours nanoparticles applied ROS Level

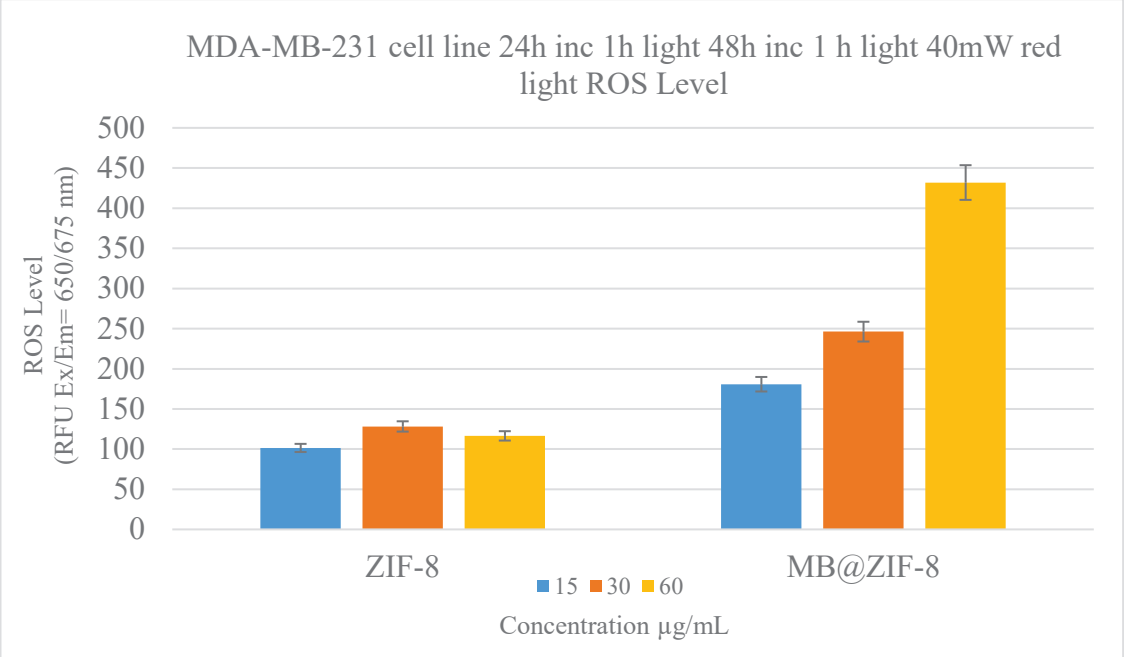

Figure 21. Effect of 60 minutes of application of 40 mW/cm^2 red light, 48-hour dark, then 60 minutes red light application again on MDA-MB-231 cell lines after 24 hours nanoparticles applied ROS Level

3.5. Apoptosis Analysis

The apoptotic effects of the synthesized ZIF-8 and MB@ZIF-8 nanoparticles on the MDA-MB-231 cell line were investigated using the FITC Annexin V Apoptosis Detection Kit with PI. Given that higher concentrations of ZIF-8 and MB@ZIF-8 nanoparticles (15, 60, and 75 µg/mL) and methylene blue dye concentrations above 7.5 µg/mL exhibited toxic effects, the study was conducted with lower concentrations of 0.15, 0.75, and 7.5 µg/mL. Following 12 and 24 hours of incubation, it was observed that apoptosis increased and cell viability decreased as the concentration increased. Additionally, apoptosis was higher after 24 hours of incubation compared to 12 hours, likely due to more significant nanoparticle accumulation and increased ROS levels.

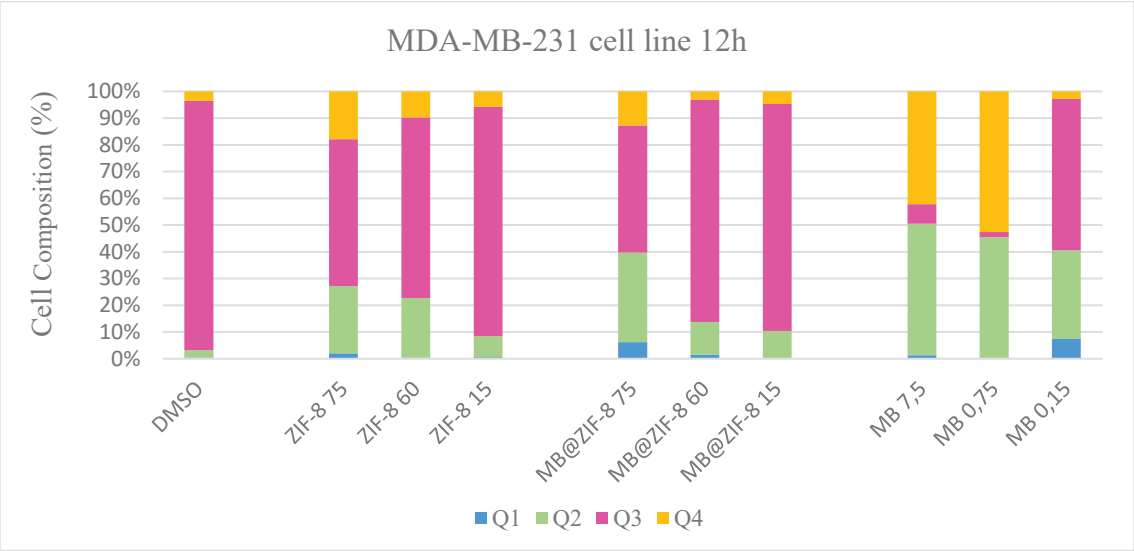

Figure 22. The apoptosis rate of nanoparticles was applied to the MDA-MB-231 cell line for 12 hours.

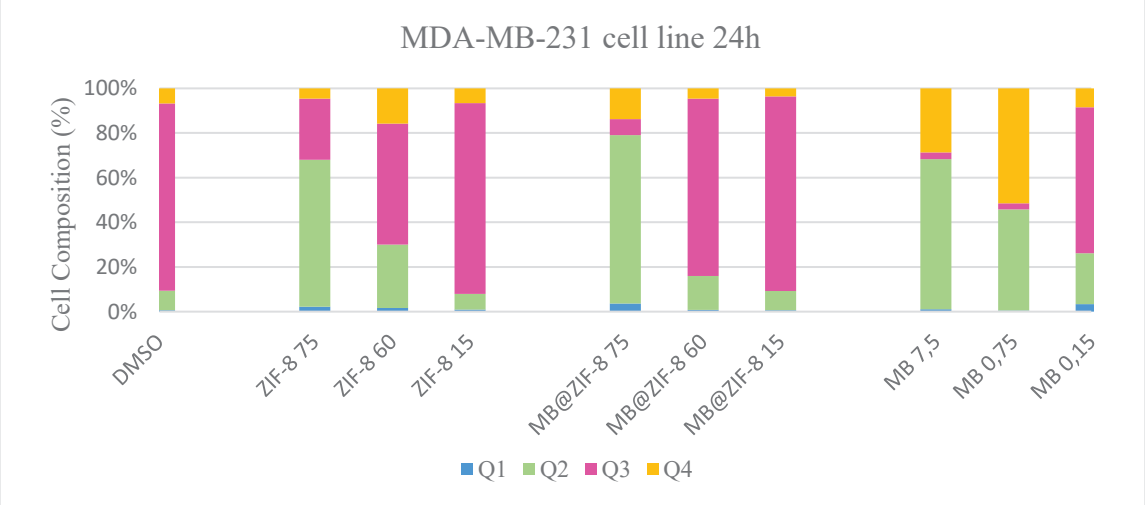

Figure 23. The apoptosis rate of nanoparticles applied to the MDA-MB-231 cell line for 24 hours.

3.6. Cell Cycle Analysis

The results of the cell cycle study revealed that DMSO, ZIF-8, MB@ZIF-8, and MB affected different cell populations in the G1, G2, and S phases in distinct ways. ZIF-8 caused a notable increase in the S phase and an elevated G2 phase population, indicating a potential cell cycle arrest at these stages. In contrast, MB@ZIF-8 significantly increased

the S phase population, suggesting a substantial impact on disrupting DNA synthesis. MB@ZIF-8 appears to be more effective than ZIF-8 in driving cells into the S phase, highlighting its potential therapeutic use in targeting rapidly dividing cells. On the other hand, MB treatment primarily resulted in a high G1 phase population, pointing to a different mechanism of cell cycle modulation. These findings suggest that MB@ZIF-8 has a significant effect on cell cycle progression, particularly in enhancing S phase arrest, which could be beneficial for therapies aimed at inhibiting DNA replication in cancer cells.

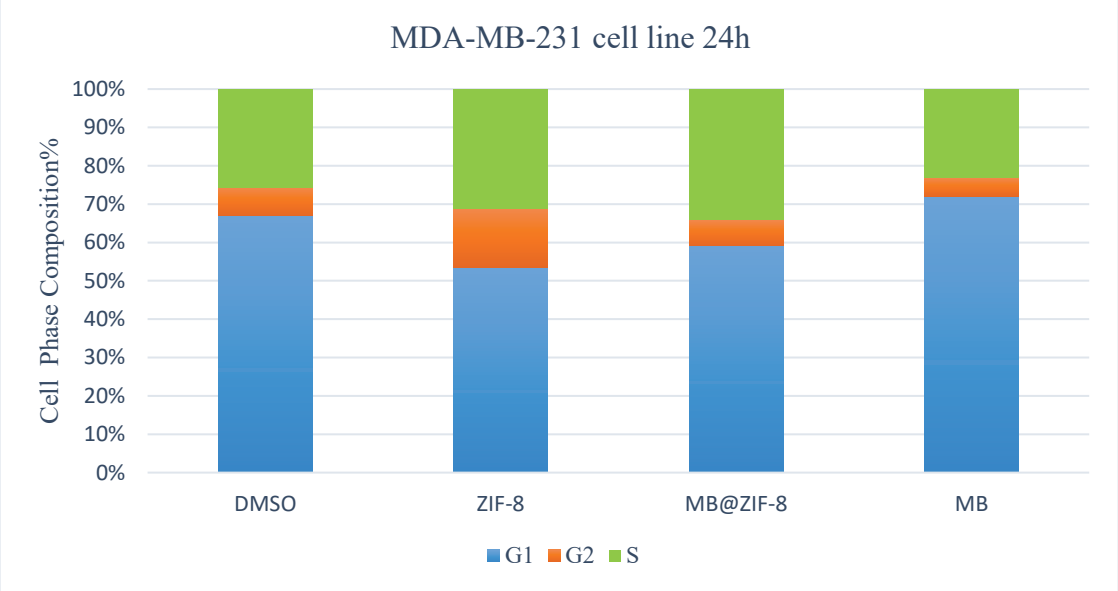

Figure 24. The MDA-MB-231 cell line's cell cycle analysis for ZIF-8, MB@ZIF-8, and MB at 24 hours

3.7. Serum Protein Binding and Hemolysis Analysis

Red blood cells, or erythrocytes, constitute approximately 48% of the blood. Hemolysis, the release of hemoglobin, is a crucial aspect of studies involving erythrocytes and metal-organic frameworks (MOFs). A hemolysis assay was conducted to investigate the percentage of erythrocyte cells in blood samples exposed to ZIF-8 and MB@ZIF-8 nanoparticles. Hemolysis rates for ZIF-8 and MB@ZIF-8 nanoparticles were tested at concentrations of 25, 50, 75 and 100 µg/Ml. At a concentration of 75 µg/mL, the hemolysis rates for ZIF-8 and MB@ZIF-8 nanoparticles were found to be 1.16% and

0.98%, respectively, as shown in Figure 25. These values, being below 5%, indicate the biocompatibility of the synthesized nanoparticles.

Following a two-hour incubation at body temperature (37°C), serum protein binding was evaluated in the presence of nanoparticles. Different serum-to-nanoparticle ratios were tested, as serum protein binding is highly individualized and can influence the overall performance of the nanoparticles. At a 70:30 serum-to-ZIF-8 ratio, the maximal binding of nanoparticles to proteins was found to be 95.98%. This high binding efficiency is important for ensuring that the nanoparticles remain effective in their intended therapeutic roles, as strong binding to serum proteins can facilitate better distribution and stability in the bloodstream.

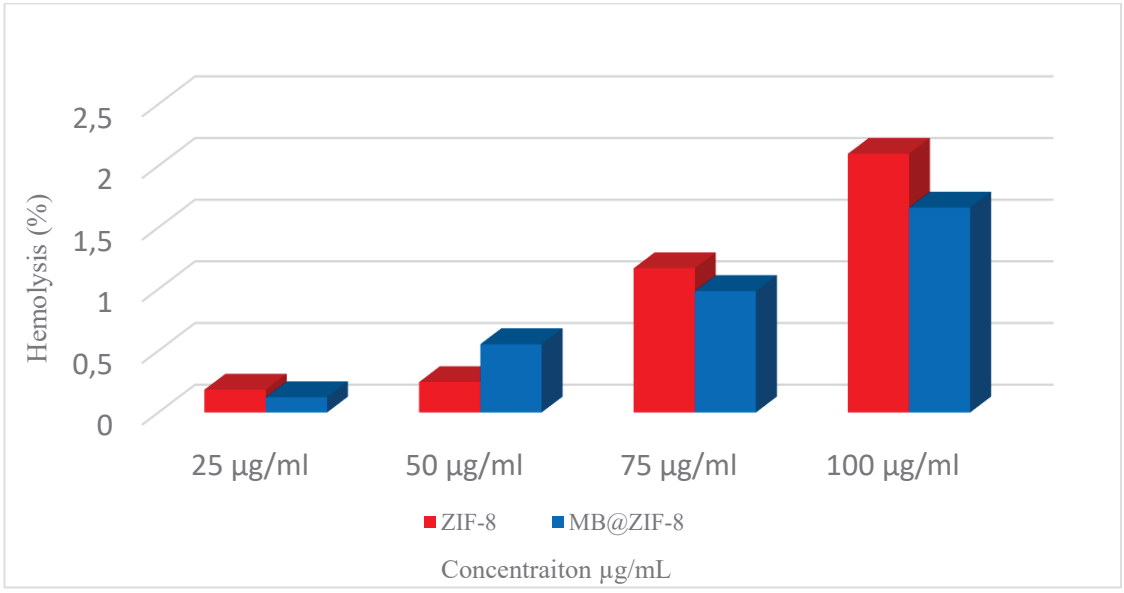

Figure 25. Hemolysis rates of ZIF-8 and MB@ZIF-8 nanoparticles

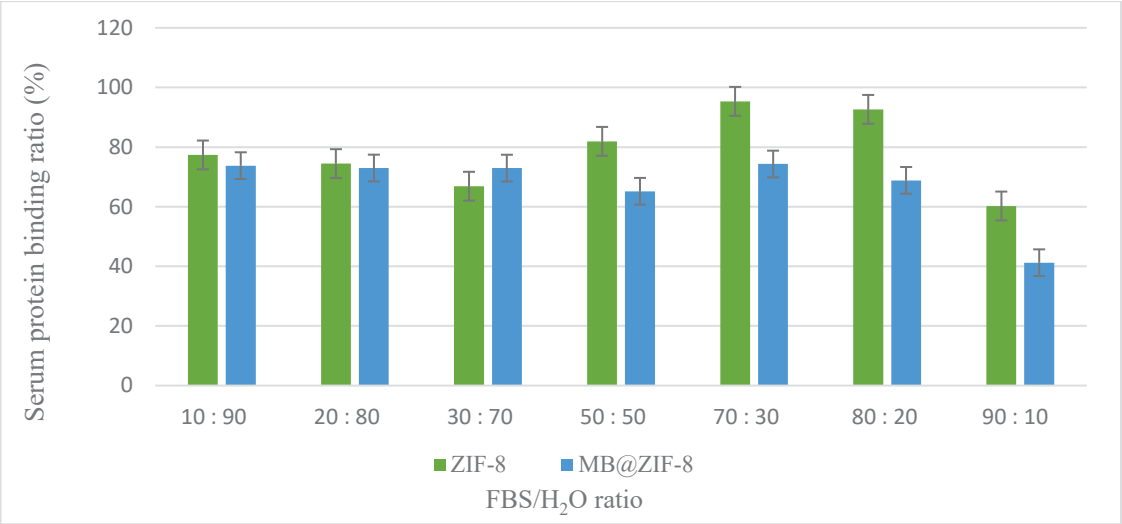

Figure 26. Serum protein ratio of ZIF-8 and MB@ZIF-8 nanoparticles

3.8. Dye Release Studies

To monitor the progress of dye release from MB@ZIF-8 nanoparticles over time, PBS buffer solutions with a normal cell pH of 7.4 and a pH 5.5 solution that simulated the acidic environment of cancer cells were created. In these two distinct pH conditions, MB@ZIF-8 nanoparticles were incubated for three days at 150 rpm. To determine how much dye was released in a given amount of time, the absorbance values of the supernatants were measured using a UV-Vis device. Figure 27. displays the total release graph obtained at pH 5.5 and 7.4. According to these findings, as previously reported, dye release from the produced nanoparticles is rapid at pH 5.5 but slower at pH 7.4. Within the first eight hours, the dye released from MB@ZIF-8 was seen to approach a release plateau at a rate of 48%, and it then continued to be released at a slower rate. Upon analyzing the dye release at pH 7.4, it was observed that the release achieved a plateau within the first 12 hours and continued to be 40% over the next three days.

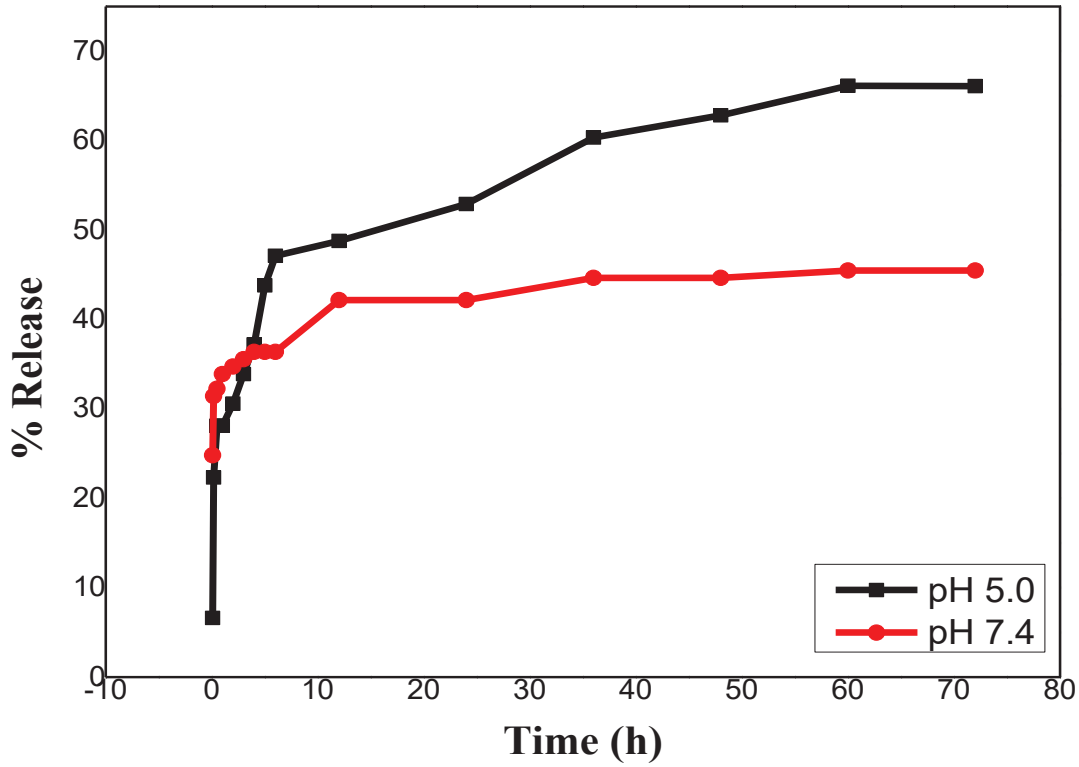

Figure 27. Dye release profiles of MB@ZIF-8 nanoparticles at pH 5.5 and 7.4

CHAPTER 4

CONCLUSION

This thesis resulted in developing a new generation smart, biocompatible, biodegradable, tumor tissue targeting, and photodynamic diagnosis and multi-functional nanocarrier system for breast cancer treatment. The system was then characterized, and its effectiveness was investigated in in vitro systems. ZIF-8 smart material has been used as an encapsulation material for Methylene blue, and its diagnostic and treatment potential for breast cancer cells has been investigated. Methylene blue is a phenothiazine dye that stands out in this field because of its strong photodynamic activity, cheapness, water solubility, and non-toxic structure.

The biocompatible ZIF-8 smart material, belonging to the metal-organic structure family, shows biodegradable qualities in acidic conditions because of the weak coordination bonds. In this study, methylene blue (MB) loaded onto ZIF-8 was released in a pH-sensitive manner, targeting cancer cells, which are more acidic than healthy cells. It was observed that the developed nanocarrier system released the photosensitizer faster in the acidic pH of the tumor microenvironment, which is lower than the physiological pH. Because of this, the system releases more photosensitizers in the cancer tissue than in the bloodstream, lowering toxicity to healthy tissues.

With the help of the chosen ZIF-8 metal-organic skeleton, the goal was to combine the effects of MB and zinc on one platform to provide a combined cytotoxic effect on breast cancer. After completing all required optimizations, the ZIF-8 nanocarrier system was synthesized using the one-pot method, and characterization investigations were performed. Zeta potential data indicated that the structure was positively charged and moderately stable, while SEM pictures revealed that the particles had been evenly distributed and that it was rhombic dodecahedral. XRD measurement was used to determine the nanoparticles' degree of crystallinity and impurity. FTIR data further validated the structure.

This study determined the optimum incubation time using the MTT assay on MCF-7 and MB-MDA-231 (human breast carcinoma) cell lines. Nanoparticles and dye-loaded nanoparticles were applied at the determined IC50 concentrations for 24 and 12

hours of incubation. Apoptotic and cell cycle stages were compared with flow cytometry to understand the suppressive functions of the drugs in cancer development. Serum and hemolysis tests were performed to evaluate the biocompatibility and reliability of the treatment methods. Apoptosis studies helped us understand the effectiveness of the treatment and its lethal effect on cancer cells by examining the programmed death processes of the cells. Cell cycle analyses were performed to determine the effects of the drugs on cell proliferation. In photodynamic therapy (PDT) experiments, the treatment was optimized by adjusting the light intensity and duration.

The results of the study show that the combination of methylene blue and photodynamic therapy can be used as a potential treatment option in breast cancer treatment. This approach aims to provide a more effective and targeted treatment for cancer cells by improving the quality of the treatment process.

REFERENCES

Abdelhamid, Hani Nasser. 2020. “Dye Encapsulated Hierarchical Porous Zeolitic Imidazolate Frameworks for Carbon Dioxide Adsorption.” *Journal of Environmental Chemical Engineering* 8 (4): 104008. https://doi.org/10.1016/j.jece.2020.104008.

Akhtar, Hamza, Umay Amara, Khalid Mahmood, Muhammad Hanif, Muhammad Khalid, Sobia Qadir, Qiaohong Peng, et al. 2024. “Drug Carrier Wonders: Synthetic Strategies of Zeolitic Imidazolates Frameworks (ZIFs) and Their Applications in Drug Delivery and Anti-Cancer Activity.” *Advances in Colloid and Interface Science* 329 (May): 103184. https://doi.org/10.1016/j.cis.2024.103184.

Alley, M C, D A Scudiero, A Monks, M L Hursey, M J Czerwinski, D L Fine, B J Abbott, J G Mayo, R H Shoemaker, and M R Boyd. 1988. “Feasibility of Drug Screening with Panels of Human Tumor Cell Lines Using a Microculture Tetrazolium Assay.” *Cancer Research* 48 (3): 589–601.

Ashkenazi, Avi, and Vishva M. Dixit. 1998. “Death Receptors: Signaling and Modulation.” *Science* 281 (5381): 1305–8. https://doi.org/10.1126/science.281.5381.1305.

Benet, Leslie Z., and Betty-Ann Hoener. 2002. “Changes in Plasma Protein Binding Have Little Clinical Relevance.” *Clinical Pharmacology & Therapeutics* 71 (3): 115–21. https://doi.org/10.1067/mcp.2002.121829.

Berridge, Michael V., Patries M. Herst, and An S. Tan. 2005. “Tetrazolium Dyes as Tools in Cell Biology: New Insights into Their Cellular Reduction.” In , 127–52. https://doi.org/10.1016/S1387-2656(05)11004-7.

Bradford, M. 1976. “A Rapid and Sensitive Method for the Quantitation of Microgram Quantities of Protein Utilizing the Principle of Protein-Dye Binding.” *Analytical Biochemistry* 72 (1–2): 248–54. https://doi.org/10.1006/abio.1976.9999.

Bray, Freddie, Jacques Ferlay, Isabelle Soerjomataram, Rebecca L. Siegel, Lindsey A. Torre, and Ahmedin Jemal. 2018. "Global Cancer Statistics 2018: GLOBOCAN Estimates of Incidence and Mortality Worldwide for 36 Cancers in 185 Countries." *CA: A Cancer Journal for Clinicians* 68 (6): 394–424. https://doi.org/10.3322/caac.21492.

Cailleau, Relda, Matilde Olivé, and Quita V. J. Cruciger. 1978. "Long-Term Human Breast Carcinoma Cell Lines of Metastatic Origin: Preliminary Characterization." *In Vitro* 14 (11): 911–15. https://doi.org/10.1007/BF02616120.

Chaffey, N. 2003. "Alberts, B., Johnson, A., Lewis, J., Raff, M., Roberts, K. and Walter, P. Molecular Biology of the Cell. 4th Edn." *Annals of Botany* 91 (3): 401–401. https://doi.org/10.1093/aob/mcg023.

Chen, Yongjun, Wei Zheng, Yingqian Li, Jieying Zhong, Jianguo Ji, and Pingping Shen. 2008. "Apoptosis Induced by Methylene-blue-mediated Photodynamic Therapy in Melanomas and the Involvement of Mitochondrial Dysfunction Revealed by Proteomics." *Cancer Science* 99 (10): 2019–27. https://doi.org/10.1111/j.1349-7006.2008.00910.x.

Denizot, François, and Rita Lang. 1986. "Rapid Colorimetric Assay for Cell Growth and Survival." *Journal of Immunological Methods* 89 (2): 271–77. https://doi.org/10.1016/0022-1759(86)90368-6.

DeSantis, Carol E., Chun Chieh Lin, Angela B. Mariotto, Rebecca L. Siegel, Kevin D. Stein, Joan L. Kramer, Rick Alteri, Anthony S. Robbins, and Ahmedin Jemal. 2014. "Cancer Treatment and Survivorship Statistics, 2014." *CA: A Cancer Journal for Clinicians* 64 (4): 252–71. https://doi.org/10.3322/caac.21235.

Dobrovolskaia, Marina A., and Scott E. McNeil. 2013. "Understanding the Correlation between in Vitro and in Vivo Immunotoxicity Tests for Nanomedicines." *Journal of Controlled Release* 172 (2): 456–66. https://doi.org/10.1016/j.jconrel.2013.05.025.

Elmore, Susan. 2007. “Apoptosis: A Review of Programmed Cell Death.” *Toxicologic Pathology* 35 (4): 495–516. https://doi.org/10.1080/01926230701320337.

Favaloro, B., N. Allocati, V. Graziano, C. Di Ilio, and V. De Laurenzi. 2012. “Role of Apoptosis in Disease.” *Aging* 4 (5): 330–49. https://doi.org/10.18632/aging.100459.

Ferlay, Jacques, Murielle Colombet, Isabelle Soerjomataram, Donald M. Parkin, Marion Piñeros, Ariana Znaor, and Freddie Bray. 2021. “Cancer Statistics for the Year 2020: An Overview.” *International Journal of Cancer* 149 (4): 778–89. https://doi.org/10.1002/ijc.33588.

Fernandez, Jim M, Mehmet D Bilgin, and Leonard I Grossweiner. 1997. “Singlet Oxygen Generation by Photodynamic Agents.” *Journal of Photochemistry and Photobiology B: Biology* 37 (1–2): 131–40. https://doi.org/10.1016/S1011-1344(96)07349-6.

Fitzmaurice, Christina, Daniel Dicker, Amanda Pain, Hannah Hamavid, Maziar Moradi-Lakeh, Michael F. MacIntyre, Christine Allen, et al. 2015. “The Global Burden of Cancer 2013.” *JAMA Oncology* 1 (4): 505. https://doi.org/10.1001/jamaoncol.2015.0735.

Forget, B. G., and H. F. Bunn. 2013. “Classification of the Disorders of Hemoglobin.” *Cold Spring Harbor Perspectives in Medicine* 3 (2): a011684–a011684. https://doi.org/10.1101/cshperspect.a011684.

Fotakis, George, and John A. Timbrell. 2006. “In Vitro Cytotoxicity Assays: Comparison of LDH, Neutral Red, MTT and Protein Assay in Hepatoma Cell Lines Following Exposure to Cadmium Chloride.” *Toxicology Letters* 160 (2): 171–77. https://doi.org/10.1016/j.toxlet.2005.07.001.

Friedrichs, B. 1997. “<scp>Th. Peters</Scp> . Jr.: All about Albumin. Biochemistry, Genetics, and Medical Applications. XX and 432 Pages, Numerous Figures and Tables. Academic Press, Inc., San Diego, California, 1996. Price: 85.00 US $.” *Food / Nahrung* 41 (6): 382–382. https://doi.org/10.1002/food.19970410631.

Furukawa, Hiroyasu, Kyle E. Cordova, Michael O'Keeffe, and Omar M. Yaghi. 2013. "The Chemistry and Applications of Metal-Organic Frameworks." *Science* 341 (6149). https://doi.org/10.1126/science.1230444.

Galluzzi, Lorenzo, Oliver Kepp, Stefan Krautwald, Guido Kroemer, and Andreas Linkermann. 2014. "Molecular Mechanisms of Regulated Necrosis." *Seminars in Cell & Developmental Biology* 35 (November):24–32. https://doi.org/10.1016/j.semcdb.2014.02.006.

Gao, Lihua, Qing Chen, Tingting Gong, Jianhua Liu, and Chunxia Li. 2019. "Recent Advancement of Imidazolate Framework (ZIF-8) Based Nanoformulations for Synergistic Tumor Therapy." *Nanoscale* 11 (44): 21030–45. https://doi.org/10.1039/C9NR06558J.

Hanahan, Douglas, and Robert A. Weinberg. 2011. "Hallmarks of Cancer: The Next Generation." *Cell* 144 (5): 646–74. https://doi.org/10.1016/j.cell.2011.02.013.

Hartwell, Leland H., and Ted A. Weinert. 1989. "Checkpoints: Controls That Ensure the Order of Cell Cycle Events." *Science* 246 (4930): 629–34. https://doi.org/10.1126/science.2683079.

Kamiloglu, Senem, Gulce Sari, Tugba Ozdal, and Esra Capanoglu. 2020. "Guidelines for Cell Viability Assays." *Food Frontiers* 1 (3): 332–49. https://doi.org/10.1002/fft2.44.

Kaur, Harpreet, Girish C. Mohanta, Vandana Gupta, Deepak Kukkar, and Sachin Tyagi. 2017. "Synthesis and Characterization of ZIF-8 Nanoparticles for Controlled Release of 6-Mercaptopurine Drug." *Journal of Drug Delivery Science and Technology* 41:106–12. https://doi.org/10.1016/j.jddst.2017.07.004.

Kerr, J F R, A H Wyllie, and A R Currie. 1972. "Apoptosis: A Basic Biological Phenomenon with Wideranging Implications in Tissue Kinetics." *British Journal of Cancer* 26 (4): 239–57. https://doi.org/10.1038/bjc.1972.33.

Key, Timothy J, Pia K Verkasalo, and Emily Banks. 2001. “Epidemiology of Breast Cancer.” *The Lancet Oncology* 2 (3): 133–40. https://doi.org/10.1016/S1470-2045(00)00254-0.

Lamberti, María Julia. 2014. “Breast Cancer as Photodynamic Therapy Target: Enhanced Therapeutic Efficiency by Overview of Tumor Complexity.” *World Journal of Clinical Oncology* 5 (5): 901. https://doi.org/10.5306/wjco.v5.i5.901.

Leon-Ferre, Roberto A., Karthik V. Giridhar, Tina J. Hieken, Robert W. Mutter, Fergus J. Couch, Rafael E. Jimenez, John R. Hawse, Judy C. Boughey, and Kathryn J. Ruddy. 2018. “A Contemporary Review of Male Breast Cancer: Current Evidence and Unanswered Questions.” *Cancer and Metastasis Reviews* 37 (4): 599–614. https://doi.org/10.1007/s10555-018-9761-x.

Ligasová, Anna, Ivo Frydrych, and Karel Koberna. 2023. “Basic Methods of Cell Cycle Analysis.” *International Journal of Molecular Sciences* 24 (4): 3674. https://doi.org/10.3390/ijms24043674.

Lubischer, J. L. 2007. “The Cell Cycle, Principles of Control. David O. Morgan.” *Integrative and Comparative Biology* 47 (5): 794–95. https://doi.org/10.1093/icb/icm066.

Mavaddat, Nasim, Susan Peock, Debra Frost, Steve Ellis, Radka Platte, Elena Fineberg, D. Gareth Evans, et al. 2013. “Cancer Risks for BRCA1 and BRCA2 Mutation Carriers: Results From Prospective Analysis of EMBRACE.” *JNCI: Journal of the National Cancer Institute* 105 (11): 812–22. https://doi.org/10.1093/jnci/djt095.

Mayer, Andrea, Maria Vadon, Beate Rinner, Alexandra Novak, Reinhold Wintersteiger, and Eleonore Fröhlich. 2009. “The Role of Nanoparticle Size in Hemocompatibility.” *Toxicology* 258 (2–3): 139–47. https://doi.org/10.1016/j.tox.2009.01.015.

Mete, Derya, Egehan Yemeztaşlıca, and Gülşah Şanlı-Mohamed. 2023. “Sorafenib Loaded ZIF-8 Metal-Organic Frameworks as a Multifunctional Nano-Carrier Offers Effective Hepatocellular Carcinoma Therapy.” *Journal of Drug Delivery Science and Technology* 82 (March). https://doi.org/10.1016/j.jddst.2023.104362.

Mosmann, Tim. 1983. “Rapid Colorimetric Assay for Cellular Growth and Survival: Application to Proliferation and Cytotoxicity Assays.” *Journal of Immunological Methods* 65 (1–2): 55–63. https://doi.org/10.1016/0022-1759(83)90303-4.

Pavlopoulou, Athanasıa, Demetrıos A. Spandıdos, and Ioannıs Mıchalopoulos. 2015. “Human Cancer Databases (Review).” *Oncology Reports* 33 (1): 3–18. https://doi.org/10.3892/or.2014.3579.

Penaloza, Carlos, Lin Lin, Richard A. Lockshin, and Zahra Zakeri. 2006. “Cell Death in Development: Shaping the Embryo.” *Histochemistry and Cell Biology* 126 (2): 149–58. https://doi.org/10.1007/s00418-006-0214-1.

Peng Chee, Tan, Ooi Boon Seng, Abdul Latif Ahmad, and Low Siew Chun. 2017. “Size Control and Stability Study of Zeolitic Imidazolate Framework-8 to Prepare Mixed Matrix Membrane.” *Journal of Physical Science* 28 (Suppl. 1): 215–26. https://doi.org/10.21315/jps2017.28.s1.14.

Pethő, Zoltán, Karolina Najder, Etmar Bulk, and Albrecht Schwab. 2019. “Mechanosensitive Ion Channels Push Cancer Progression.” *Cell Calcium* 80 (June):79–90. https://doi.org/10.1016/j.ceca.2019.03.007.

Prasad, Ananda S., Frances W. J. Beck, Diane C. Snell, and Omer Kucuk. 2009. “Zinc in Cancer Prevention.” *Nutrition and Cancer* 61 (6): 879–87. https://doi.org/10.1080/01635580903285122.

Provinciali, Mauro, Elisa Pierpaoli, Beatrice Bartozzi, and Giovanni Bernardini. 2015. “Zinc Induces Apoptosis of Human Melanoma Cells, Increasing Reactive Oxygen Species, P53 and FAS Ligand.” *Anticancer Research* 35 (10): 5309–16.

Rahimipour, Shai, Nurit Ben-Aroya, Keren Ziv, Alon Chen, Mati Fridkin, and Yitzhak Koch. 2003. “Receptor-Mediated Targeting of a Photosensitizer by Its Conjugation to Gonadotropin-Releasing Hormone Analogues.” *Journal of Medicinal Chemistry* 46 (19): 3965–74. https://doi.org/10.1021/jm020535y.

Rakha, Emad A., Maysa E. El-Sayed, Desmond G. Powe, Andrew R. Green, Hany Habashy, Matthew J. Grainge, John F.R. Robertson, et al. 2008. “Invasive Lobular Carcinoma of the Breast: Response to Hormonal Therapy and Outcomes.” *European Journal of Cancer* 44 (1): 73–83. https://doi.org/10.1016/j.ejca.2007.10.009.

Richie, Rodney C, and John O Swanson. 2003. “Breast Cancer: A Review of the Literature.” *Journal of Insurance Medicine (New York, N.Y.)* 35 (2): 85–101.

Romanello, Marina, Alice McGushin, Claudia Di Napoli, Paul Drummond, Nick Hughes, Louis Jamart, Harry Kennard, et al. 2021. “The 2021 Report of the Lancet Countdown on Health and Climate Change: Code Red for a Healthy Future.” *The Lancet* 398 (10311): 1619–62. https://doi.org/10.1016/S0140-6736(21)01787-6.

Rowsell, Jesse L.C., and Omar M. Yaghi. 2004. “Metal–Organic Frameworks: A New Class of Porous Materials.” *Microporous and Mesoporous Materials* 73 (1–2): 3–14. https://doi.org/10.1016/j.micromeso.2004.03.034.

Santos, Ancély F. dos, Letícia F. Terra, Rosangela A. M. Wailemann, Talita C. Oliveira, Vinícius de Morais Gomes, Marcela Franco Mineiro, Flávia Carla Meotti, Alexandre Bruni-Cardoso, Maurício S. Baptista, and Leticia Labriola. 2017. “Methylene Blue Photodynamic Therapy Induces Selective and Massive Cell Death in Human Breast Cancer Cells.” *BMC Cancer* 17 (1): 194. https://doi.org/10.1186/s12885-017-3179-7.

Sherr, C. J., and J. M. Roberts. 1999. “CDK Inhibitors: Positive and Negative Regulators of G1-Phase Progression.” *Genes & Development* 13 (12): 1501–12. https://doi.org/10.1101/gad.13.12.1501.

Skıpper, H E, F M Schabel, and W S Wılcox. 1964. “Experımental Evaluatıon Of Potentıal Antıcancer Agents. Xııı. On The Crıterıa and Kınetıcs Associated Wıth ‘Curabılıty’ Of Experımental Leukemıa.” *Cancer Chemotherapy Reports* 35 (February):1–111.

Soule, H. D., J. Vazquez, A. Long, S. Albert, and M. Brennan. 1973. “A Human Cell Line From a Pleural Effusion Derived From a Breast Carcinoma 2.” *JNCI: Journal of the National Cancer Institute* 51 (5): 1409–16. https://doi.org/10.1093/jnci/51.5.1409.

Strasser, Andreas, Liam O’Connor, and Vishva M. Dixit. 2000. “Apoptosis Signaling.” *Annual Review of Biochemistry* 69 (1): 217–45. https://doi.org/10.1146/annurev.biochem.69.1.217.

Subhan, Md Abdus, Satya Siva Kishan Yalamarty, Nina Filipczak, Farzana Parveen, and Vladimir P. Torchilin. 2021. “Recent Advances in Tumor Targeting via EPR Effect for Cancer Treatment.” *Journal of Personalized Medicine* 11 (6): 571. https://doi.org/10.3390/jpm11060571.

Tait, Stephen W. G., and Douglas R. Green. 2010. “Mitochondria and Cell Death: Outer Membrane Permeabilization and Beyond.” *Nature Reviews Molecular Cell Biology* 11 (9): 621–32. https://doi.org/10.1038/nrm2952.

Tenhunen, Tiia-Maria, Anna E. Lewandowska, Hannes Orelma, Leena-Sisko Johansson, Tommi Virtanen, Ali Harlin, Monika Österberg, Stephen J. Eichhorn, and Tekla Tammelin. 2018. “Understanding the Interactions of Cellulose Fibres and Deep Eutectic Solvent of Choline Chloride and Urea.” *Cellulose* 25 (1): 137–50. https://doi.org/10.1007/s10570-017-1587-0.

Tyrrell, Jessica, Cheryl Paterson, and Alison Curnow. 2019. “Regression Analysis of Protoporphyrin IX Measurements Obtained During Dermatological Photodynamic Therapy.” *Cancers* 11 (1): 72. https://doi.org/10.3390/cancers11010072.

Vousden, Karen H., and David P. Lane. 2007. “P53 in Health and Disease.” *Nature Reviews Molecular Cell Biology* 8 (4): 275–83. https://doi.org/10.1038/nrm2147.

Wang, Jianjun, Zhiyong Gao, Yuesheng Gao, Yuehua Hu, and Wei Sun. 2016. “Flotation Separation of Scheelite from Calcite Using Mixed Cationic/Anionic Collectors.” *Minerals Engineering* 98 (November):261–63. https://doi.org/10.1016/j.mineng.2016.09.006.

Xin, Yanru, Mingming Yin, Liyuan Zhao, Fanling Meng, and Liang Luo. 2017. “Recent Progress on Nanoparticle-Based Drug Delivery Systems for Cancer Therapy.” *Cancer Biology & Medicine* 14 (3): 228. https://doi.org/10.20892/j.issn.2095-3941.2017.0052.

Zou, Dianting, Dingxin Liu, and Jianyong Zhang. 2018. “From Zeolitic Imidazolate Framework-8 to Metal-Organic Frameworks (MOFs): Representative Substance for the General Study of Pioneering MOF Applications.” *Energy and Environmental Materials* 1 (4): 209–20. https://doi.org/10.1002/eem2.12018.